RNA Targets and Physiological Role of Topoisomerase 3β

Shohreh Teimuri and Beat Suter*

Institute of Cell Biology, University of Bern, Berne, 3012, Switzerland

*Corresponding address: Beat.Suter@unibe.ch

Keywords: Topoisomerase 3β, Drosophila, RNA topoisomerase targets, posttranscriptional gene expression, cellular stress, neurodegeneration, cancer.

Short title: RNAs targets of Topoisomerase 3β

Abstract

Topoisomerase 3β (Top3β) works not only on DNA but also RNA. We isolated and identified the naturally cross-linked RNA targets of Drosophila Top3β from an early embryonic stage that contains almost exclusively maternal mRNAs. Favorite targets were longer RNAs, RNAs with many splice sites, and RNAs that become localized in large cells. Demonstrating the importance of its enzymatic activity, Top3β without the hydroxyl group that makes the covalent bond to the RNA, did not allow normal expression and subcellular localization of tested gene products of the identified targets. *Top3β* is not essential for development to the adult stage but to maintain the morphology of the neuromuscular junction in adult flies and to prevent premature loss of coordinated movement and aging. Alterations in human *Top3β* have been associated with several neurological diseases and cancers. The homologs of genes and (pre)mRNAs mis-expressed in these conditions show the same characteristics identified in the Drosophila *Top3β* targets, suggesting that Drosophila could model the function of human *Top3β*. Indeed, an *in vivo* test of this model showed that the enzymatic activity of Top3β reduces the neurodegeneration caused by the human $(G4C2)_{49}$ RNA. Together, these studies show that *Top3β* plays important roles in normal gene expression, particularly for large genes and long and complex transcripts that need to be transported and translationally controlled. Its absence stresses the cells, seemingly increasing the chances of contracting various neuronal and neurodegenerative diseases and cancers.

41 ## Introduction

42 Topoisomerase 3β (Top3β) is an RNA-binding protein (RBP) with dual enzymatic activity
43 toward DNA and RNA (1) (88). Topoisomerases are better known for their activity toward
44 DNA, where they resolve tension and supercoiling, a prerequisite for efficient transcription,
45 transcription control, and replication (11) (86) (recently also reviewed in 87). Much less is
46 known about the function of topoisomerases toward RNA. Along with other RBPs, Top3β
47 interacts with the RNAi machinery (49), and it contributes to mRNA stability and translation,
48 particularly in the nervous system, which is significant for neurodevelopment and
49 psychological and physical well-being (2)(74)(85). Its functional importance is suggested by
50 results that link impaired *Top3β* function to various neurodevelopmental and cognitive
51 disorders (2)(3)(73)(84).

52 *Drosophila melanogaster* Top3β possesses the key features of a topoisomerase. The
53 predicted catalytic tyrosine (Tyr, Y; (4) (90)) residue is present at position 332 (Y332). Top3β
54 topoisomerases distinguish themselves from other topoisomerases by their conserved RNA-
55 binding motif called RGG (Arginine Glycine Glycine) box, which binds to RNAs or proteins. Its
56 paralogue Top3α, a DNA topoisomerase, possesses the catalytic tyrosine residue but lacks the
57 RGG box (4). *In vitro*, the RGG box is not required for the enzymatic activity but might play a
58 role in binding to the RNA and thereby facilitating the enzymatic activity *in vivo* (2).

59 We hypothesized that the neurological requirements for an RNA topoisomerase may in part
60 reflect its activity on mRNAs that need to be transported over long distances to be
61 translated at the right place and time. During such transport, long molecules, such as
62 mRNAs, are likely to become entangled or suffer other structural problems that might
63 interfere with their packaging, transport, unpackaging, and translation (1)(94). Therefore, a

64 topoisomerase that acts on RNAs might be able to rescue such RNAs. As discussed by Su and
65 colleagues (74), there is considerable evidence that Top3β activity on RNA has important
66 functions in cells and that it might act at all levels of gene expression. Using human cell
67 lines, these authors showed that Top3β indeed affects mRNA translation and RNA stability
68 (74). They also found evidence that these effects involve mainly TDRD3, which could be
69 strengthened by the recently described mouse *Tdrd3*-null phenotype (85). However, there is
70 still surprisingly little knowledge about the steps in gene expression where Top3β acts on
71 RNAs and particularly about the *in vivo* role of this activity for the cells and the organism.
72 Especially in large cells, where mRNAs need to travel over long distances, an RNA
73 topoisomerase could provide an important advantage and allow the cell to function
74 properly. Drosophila has such large cells in the nervous system, the female germline, and
75 the young, syncytial embryo. The latter is easily accessible and free of additional tissue.
76 According to Flybase (https://flybase.org/reports/FBgn0026015), the expression of
77 Drosophila Top3β is particularly abundant in 0-2 hours old embryos, when the syncytial
78 embryos are in the first 10 nuclear divisions cycles (78). The mRNAs in these large cells are
79 maternally provided and bulk zygotic transcription would only start about an hour later,
80 around cellularizations (reviewed by (79), (80)).

81 Proper mRNA localization to specific compartments combined with controlled local
82 translation is essential for normal differentiation and cellular physiology and it has been
83 studied extensively during these stages. This developmental stage, therefore, appears to
84 provide a unique opportunity to study the activity and function of Drosophila Top3β toward
85 cytoplasmic RNAs by identifying relevant *in vivo* RNA targets.

86 Here we show that in such 0-2 hours old embryos, longer RNAs were more frequently bound
87 to Top3β in a Y332-dependent way. This is consistent with the notion that larger RNAs are
88 more likely to encounter structural problems that are being targeted and repaired by the RNA
89 topoisomerase in living cells. The same RNA features are also over-represented among the
90 differentially expressed RNAs in the *Top3β* mutants. As opposed to the capturing of the
91 targets in young, preblastoderm embryos, the transcriptomics analysis is expected to reveal
92 the sum of direct and indirect effects of the cytoplasmic and the nuclear activities of Top3β.
93 Specific mutations of the Y332 active site tyrosine (Y332F) and the RGG box (ΔRGG) revealed
94 the importance of the enzymatic and RNA/protein binding activity, respectively. The
95 enzymatic activity of Top3β is needed to covalently bind to mRNAs and for the normal
96 accumulation of many long mRNAs and their encoded proteins in general, and also in specific
97 subcellular locations. The lack of this enzymatic activity is not essential for the viability of the
98 embryos or larvae but stresses the affected cells and causes neurodegeneration and
99 premature aging of adults. Because the Drosophila enzyme affects the outcome of a human
100 RNA that causes neurodegeneration, this Drosophila model produces valuable novel insights
101 into neurodegenerative diseases and cancers with which human *Top3β* had been associated.

102

103 ## Results

104 ### RNAs depending on *Top3β* for their normal expression

105 To test whether Top3β affects gene expression at the RNA level, RNAs from 0-2 hours-old
106 embryos were extracted from a wild-type control strain and the *Top3β* mutants $Top3\beta^{26}$, a
107 null mutant (49)(50) caused by a deletion of a large fraction of the coding sequence starting
108 at codon Y141 and changing it into a stop codon, $Top3\beta^{Y332F}$, and $Top3\beta^{\Delta RGG}$, point mutants
109 generated for this work to test the function of Y332 and the RGG motives. All mutants were
110 both maternally and zygotically mutant. Sequence analysis of the transcriptome carried out
111 on biological triplicates established the effect of the different *Top3β* mutations on the RNA
112 levels expressed in 0-2 hours old embryos (**Supplementary Table S1-3; Supplementary Fig.**
113 **S1**). Using adjusted p-values (Adjp) <0.05 and log2 fold changes <-1 and >1, RNAs that showed
114 level changes between the mutant and the wild-type strains were selected for a first analysis
115 (**Fig. 1A,** left and central panel). Much more stringent conditions (Adjp <0.0002 and log2 fold
116 changes <-1) were also used (**Fig. 1A,** right panel). In both analyses, the strongest effect was
117 observed with the null mutant $Top3\beta^{26}$ which also displayed a very strong reduction of the
118 $Top3\beta^{26}$ RNA levels (**Supplementary Table S1; Supplementary Fig. S1).** As opposed to the null
119 mutant, the RNA with the point mutation was stable **(Supplementary Tables S2-3)**. The gene
120 ontology analysis of biological processes revealed similar results for $Top3\beta^{Y332F}$ and $Top3\beta^{26}$,
121 but no enrichment terms for $Top3\beta^{\Delta RGG}$ (**Supplementary Fig. S2).** The affected processes
122 range mainly from morphogenesis, synapse signaling, and trans-membrane transport to cell
123 adhesion and cuticle formation. Several of these processes are active repeatedly in the life
124 cycle, and this includes neurons and their synapses.

125 Only a small fraction of the affected genes displayed upregulation in the mutants (**Fig. 1A;**
126 **Supplementary Fig. S3**). The majority were downregulated. The downregulated genes still
127 showed a high overlap between the point mutations and the null mutant, indicating that the
128 point mutations act as (partial) loss-of-function mutations. 92% and 85%, respectively, of the
129 effects seen with the Y332F mutant using the Adjp <0.05 and Adjp <0.0002, respectively, were
130 also observed with the null mutant. This points to the importance of the active site Tyrosine
131 (Y332) for the function of Top3β and indicates that the enzymatic activity is important for the
132 proper expression levels of many genes. The strong overlap with the null mutant is also
133 reassuring because the two mutants are from different genetic backgrounds. In contrast, the
134 *Top3β*$^{\Delta RGG}$ mutation was induced in the same genetic background as the *Top3β*^{Y332F} mutation.
135 The fact that with both thresholds only 11% of the *Top3β*^{Y332F} hits were also identified in the
136 *Top3β*$^{\Delta RGG}$ mutant shows that strain background differences do not, or only weakly, affect the
137 data quality.

138 Large genes tend to produce more frequently different mRNA isoforms, sometimes with
139 different protein-coding capacities and even functions. With the standard expression profiling
140 used so far, we might miss a strong effect on one isoform if other mRNA isoforms are not
141 affected or compensate for the missing one. To find out whether *Top3β* is needed to produce
142 normal levels of specific mRNA isoforms, we allocated the sequence hits to specific transcripts
143 using the Salmon method (91) (**Supplementary Tables S4-S7, Fig. 1B**). The expression levels
144 of individual transcript isoforms were then compared between the null mutant and the wild
145 type using as cut off Adjp <0.05 and absolute log2 fold changes ≥1. This yielded 677
146 differentially expressed RNAs of which 67% (453) were downregulated (and 224 upregulated)
147 in the null *Top3β*^{26} mutant, suggesting again that *Top3β* is mainly needed for the production
148 or stability of RNAs. The transcript isoforms that are upregulated in the mutant, might either

149 be direct targets or generated by indirect, e.g., compensatory effects. A closer inspection
150 revealed that many genes with a transcript species that was upregulated in the mutant had a
151 different isoform that was downregulated in the same mutant. This is consistent with a
152 compensatory mechanism and a genomic background effect, but also with the lack of Top3β
153 affecting splicing, polyadenylation site selection, or promoter usage, causing the expression
154 to shift to a different RNA isoform.

155 We next investigated the contribution of the catalytic Tyr, which is essential for the enzymatic
156 activity, and the RGG motives, which mediate interactions with RNAs and proteins, toward
157 the expression of specific transcript isoforms. To reduce strain-specific and random effects,
158 we used the same cut-off values as before and focused on the 677 genes that are differentially
159 expressed in the null mutant. As shown in **Fig. 1B**, close to half (43%) of the transcript isoforms
160 identified in the null mutant were also identified as differentially expressed in the *Top3β*^{Y332F}
161 mutant (**Supplementary Table S7**). In the *Top3β*^{Y332F} mutant, 211 out of 289 (73%)
162 differentially expressed RNAs were downregulated in the embryos, suggesting that the
163 enzymatic function acts mainly to support RNA expression. Furthermore, this fraction is close
164 to the 67% observed in the null mutant, indicating that the catalytic mutant has similar effects
165 on the transcriptome of 0-2 hours old embryos as the null mutant. The impact of the mutated
166 RGG domain on the embryonic transcriptome was less pronounced, with 29 out of 61 (47%)
167 RNAs downregulated in the embryo, many might be indirect targets. Remarkably, 20 of these
168 29 RNA isoforms depended not only on the RGG motives of Top3β but also on the Y332 for
169 their normal expression levels **(Fig. 1B)**. Changes in mRNA levels in 0-2 hours old embryos of
170 *Top3β* mutants are not only due to a combination of direct and indirect effects of a specific
171 mutation but also reflect the combined effects of the Top3β activity on the DNA of the nurse

172 cells during oogenesis and on the pre-mRNAs and the mRNAs during oogenesis and
173 embryogenesis.

174 We next selected from the list of preselected transcript isoforms **(Supplementary Table S7)**
175 the 50 that showed the strongest reduction (according to their log2fc) in the null mutant and
176 the Y332F mutant, and the top 5 for ΔRGG that were also in the top list of the null mutant.
177 We then asked which RNA features were overrepresented in this group compared to the wild-
178 type control. Selecting the top hits should reveal with higher confidence gene- and RNA
179 features requiring *Top3β* activity to reach normal expression levels. On the other hand, many
180 RNAs that appeared interesting according to the volcano blots were not included anymore
181 (**Supplementary Fig. S1**). In embryos, the RNAs that were less expressed in the $Top3\beta^{Y332F}$ and
182 $Top3\beta^{26}$ mutants had longer untranslated regions (UTRs), protein-coding sequences (CDS),
183 and pre-mRNAs (**Fig. 1C-1E**). We conclude that long pre-mRNAs and mRNAs depend more
184 strongly on *Top3β* to reach their normal expression levels.

185 The analysis of the significant changes in transcript isoform levels (**Supplementary Table S7)**
186 revealed that at least 49 genes with reduced RNA levels of one isoform had at least one other
187 isoform that was significantly higher expressed. Because these pairs might help to reveal the
188 mode of action of *Top3β*, we studied 20 reciprocally expressed isoform pairs (**Supplementary**
189 **Table S14**). In 11 cases, the upregulated transcript isoforms started more upstream, 3 further
190 downstream, and 6 at the same location. The latter group displayed alternative and additional
191 splicing and 3'end formation. Top3β is a good candidate for modulating such splicing
192 activities. Due to the different start locations observed in 14 cases, the pairs with the different
193 transcription start sites differed in their 5'UTR and sometimes in the N-term of the ORF, too.
194 Additionally, differences in splicing and splice site selection were also observed. Some pairs

195 displayed different protein-coding capacities while others did not. The *Shaker cognate l-RA*
196 (*ShaI-RA*) isoform was present at higher levels in the *Top3β* null and Y332F mutants, but
197 contains a shorter last intron, causing earlier translation termination and lack of C-terminal
198 parts of the voltage-gated K-channel. *ShaI* is involved in neuronal physiology, locomotion, and
199 lifespan. Another example of strong differences between the pairs of mRNA isoforms was
200 found in *Tropomyosin-1 (TM1*). Apart from 3'UTRs of different lengths, excision of a part of
201 the 5'UTR, and different inclusions of small exons, the transcripts *TM1-RM* and *TM1-RA* start
202 far apart and show very different alternative splicing patterns such that a large fraction of
203 their ORF stems from different parts of the gene. Even though topoisomerases are involved
204 in remodeling chromatin, the upregulation of transcript isoforms that initiate at different sites
205 could also be the product of more indirect effects that compensate for the lack of another
206 isoform.

207

208 ***Top3β* in neurological diseases and cancers**

209 *Top3β* has been associated with several neurological diseases and cancers in humans. To test
210 whether the human *Top3β* might similarly act to support the expression of higher levels,
211 particularly of long RNAs, a list of diseases associated with *Top3β* was retrieved using gene-
212 disease associations (DisGeNET (v7.0)(5)). The 12 diseases identified were either neurological
213 diseases or cancers. The lists of differentially expressed genes associated with each of these
214 diseases were then obtained from the same database and used to identify their *Drosophila*
215 orthologues from DIOPT Version 9.0 (**Supplementary Table S8**). The list of these *Drosophila*
216 genes was then compared with the list of transcript isoforms (and their genes) whose
217 embryonic mRNA levels were reduced in the absence of *Top3β* (**Supplementary Table S7**). A

218 sizable fraction of the 453 genes encoding *Top3β*-dependent isoforms, were also Drosophila
219 orthologs of genes affected by these neurological diseases and cancers (**Fig. 2**). Due to the
220 small number of genes affected in the Juvenile Myoclonic Epilepsy (JME), this disease was not
221 considered for further studies. For the remaining ones, there is a clear overlap between the
222 two datasets and the overlap ranges between 2 and >3 times the calculated random overlap,
223 suggesting that the effects seen in the fly model with the inactivated *Top3β* also contribute
224 to the human disease phenotype.

225 Notably, a single gene, *Rop* (*Ras opposite*), was present in the lists from all neurological
226 diseases and the downregulated embryonic RNA isoforms (**Fig. 2C**). *Rop,* is involved in vesicle
227 release and control of synaptic activity (6)(7). In contrast, comparing all cancer lists with the
228 downregulated embryonic RNAs in the *Top3β* mutants, revealed 50 genes shared between
229 the six different lists (**Figs. 2D, E**). Their KEGG pathway analysis indicated their involvement in
230 the MAPK (mitogen-activated protein kinase) signaling pathway that regulates various cellular
231 processes, including cell growth, proliferation, differentiation, and survival (8) (9). Thus, it
232 seems that the MAPK signaling pathway is particularly sensitive to *Top3β* inactivation.

233 We also compared the features of the Drosophila RNAs shared between the data sets in **Figs.**
234 **2A, B** and compared them with the ones present only in the human disease-derived list or the
235 fly list of embryonic RNAs that depend on *Top3β* **(Supplementary Fig. S4**). With the exception
236 of JME, the RNAs shared between the two datasets had on average longer 3' and 5' UTRs than
237 the orthologs of the human disease RNAs that were not in the *Top3β*-dependent dataset.
238 Similarly, in most cases, the pre-mRNAs in the overlapping group were significantly longer.
239 This result is consistent with the human *Top3β* also affecting the expression of RNAs with the
240 same features as its fly homolog, pointing to the potential value of identifying direct Top3β

241 target mRNAs in the model system because their reduced expression might contribute to the
242 disease phenotype.

243

244 ***In vivo* RNA interactions of Top3β in the absence of bulk transcription**

245 By capturing mRNA targets directly during the first 2 hours of embryogenesis, we should be
246 able to focus on direct RNA targets of Top3β and avoid indirect effects. Furthermore, because
247 this time window ends before zygotic transcription takes off, we do not expect Top3β to bind
248 to pre-mRNAs in this assay and we should be able to focus on cytoplasmic interactions. To
249 identify directly the RNA targets to which Top3β binds and performs its topoisomerase
250 activity, we sequenced the RNAs attached to Top3β::eGFP by immunoprecipitation (IP) in the
251 presence of limited amounts of ionic detergents. This was done using animals that expressed
252 an eGFP fused to wild-type Top3β and, as a negative control, Top3β^{Y332F}::eGFP in which Y332
253 was replaced by a phenylalanine (Y332F). This mutant form of Top3β lacks only the -OH group
254 through which Top3β forms the transient covalent bond between its Y332 side chain and the
255 RNA target during the enzymatic reaction (10). We confirmed by qMS analysis that the wild-
256 type and the mutant Top3β::eGFP fusions were expressed at similar levels **(Supplementary**
257 **Table S9**). The naturally occurring covalent bond between Top3β and its targets makes
258 artificial cross-linking superfluous (thus reducing the problem of high background) while
259 allowing the use of ionic detergents at low concentrations during the isolation. These
260 conditions should pull down primarily covalently bound RNAs without denaturing the
261 antibodies and their interactions. Because we expected that only a small fraction of the
262 potential targets would be bound at the time of tissue lysis, we tried to preserve the covalent
263 bond between Top3β's Y332 and the RNA targets for the IP by complexing Mg^{2+}, which is

264 needed for the enzyme to resolve the bond at the end of the enzymatic reaction (11)(90). To
265 determine if the target RNAs were specifically bound to the –OH group of Y332, we used the
266 Y332F mutant as a negative control as described above. The RNAs that are enriched in the
267 Top3β^{+}::eGFP (Top3β::eGFP) IP compared to the Y332F mutant are candidate targets of the
268 catalytic activity of Top3β **(Supplementary Table S10)**. Because long RNAs seem more likely
269 to depend on this enzymatic activity, we further tested the quality of the data by comparing
270 the RNA length of the presumed targets with the background RNA length. Indeed, longer
271 RNAs were more likely to covalently bind to Top3β as they showed higher enrichment in IPs
272 from embryonic extracts containing Top3β::eGFP compared to the Top3β^{Y332F}::eGFP control
273 (**Fig. 3A**). It appears possible that a minor fraction of the suspected target RNAs represents
274 false positives if their expression is upregulated by Top3β::eGFP but not by Top3β^{Y332F}::eGFP
275 expression. However, such an effect would not be expected to lead to the size correlation
276 observed **(Fig. 3A)**. This argues that if such an effect exists, it would be only a minor one. The
277 size correlation results might also reflect that longer RNAs have a higher chance of enduring
278 physical stress and are, also for this reason, more likely to become substrates of the enzymatic
279 activity of Top3β. Interestingly, recent work in human cells also found that TOP3β
280 preferentially binds to long mRNAs (74).

281 From the list of immunopurified RNAs, the ones with an adjusted p-value smaller than 0.05
282 (adjp-value<0.05) and a log2-fold change of more than 1 (log2FC>1) were selected and ranked
283 based on their adjp-value. We used these parameters primarily because it is difficult to
284 capture the covalently bound phase. We noted that *Rop* was close to the cut-off with an adjp-
285 value of 0.027 and a log2-fold change of 0.54 (**Supplementary Table S10**). 46 embryonic RNAs
286 and their genes fulfilled these criteria and were used for further analyses (**Supplementary**
287 **Table S11**). The features that these RNAs share, can either indicate features that increase the

288 chance of becoming a target of the enzymatic activity of Top3β or correlate with another
289 feature that increases the chance of becoming a target. Drosophila embryonic Top3β RNA
290 targets displayed on average a higher number of transcript isoforms and exons per gene, and
291 longer 3'- and 5'UTRs compared to the complete set of different types of RNAs detected in
292 the Top3β^{+}::eGFP IPs (**Figs. 3B-D, Supplementary Tables S10-S11)**. The fact that targeted
293 mRNAs have longer 3'UTRs is consistent with mRNAs that undergo localization and/or
294 translational regulation having a higher chance of becoming a Top3β target because these
295 processes are mainly controlled by sequences in the 3'UTR. A higher abundance of mRNAs
296 with long coding sequences (CDS) might reflect that mRNAs with long open reading frames
297 (ORFs) might become a Top3β target when their translation stalls (**Fig. 3E, Supplementary**
298 **Tables S10-S11)**. Whereas the longer introns and the higher number of exons might indicate
299 that mRNA splicing increases the chance of becoming a Top3β target, the absence of
300 transcription in the first two hours of embryogenesis seems to argue that these mRNAs are
301 more likely to become targets because of other criteria that also apply to this group of genes.
302 In summary, these results present evidence for the involvement of Top3β with long and
303 complex mRNAs and mRNAs that are localized and/or under translational control. This is also
304 consistent with a reported finding that long mRNAs are overrepresented among human
305 mRNAs artificially crosslinked to Top3β in tissue culture cell lines (74).

306

307 **Connecting the Drosophila Top3β data to mammalian Top3β, FMR1, and FMRP**

308 The Drosophila proteins copurifying with Top3β::GFP support its suggested roles in
309 translation, interacting with cytoplasmic RNAs and RNP granules (**Supplementary Table S9;**
310 **Supplementary Fig. S5**). The interaction network shows that one branch of its interactions

311 goes through Tdrd3 and FMR1, the fly homolog of the fragile X mental retardation syndrome
312 protein (FMRP) (**Supplementary Fig. S5B**). Mammalian Top3β has been linked to FMRP, too,
313 and it binds to ribosomes and regulates translation (1). These researchers also found an
314 overlap between HITS-CLIP data produced with FMRP and mouse brain extracts and Top3β
315 HITS-CLIP data obtained with Flag-Top3β and HeLa extracts. Comparing the Drosophila
316 Top3β::eGFP RNA-IP results with the shared mammalian result set, revealed that homologs
317 of 12 of the 46 top maternal embryonic Drosophila targets were also present in the combined
318 mammalian list. Considering that data not only from different species but also from different
319 tissues were compared, this strong overlap reveals mRNA targets that support mainly cellular
320 physiology in different cell types (**FIG. 4A**). These results further strengthen the value of the
321 technique applied to obtain the Drosophila Top3β target RNAs and the use of Drosophila as a
322 model to study the role of Top3β in human disease. The common feature of the proteins
323 encoded by the shared RNA targets is that they are predominantly large proteins. Many are
324 localized to the plasma membrane or the cell cortex (e.g., Sev, Mgl, α-Spec, Kst, Pcx) or
325 cytoskeleton-associated (e.g., Dhc64C, Mhc, Myo10A, α-Spec, Kst), have axonal functions
326 (e.g., Shot, Dhc64C, Kst, Prosap), or scaffolding functions (Shot, Prosap). Consistent with
327 similar results in vertebrates (74), these results show that there is a clear overlap between
328 the Top3β and the FMRP activities but, additionally, the two proteins might perform activities
329 independently of the other one.

330 We also compared the effects of Drosophila *Top3β* and *FMR1* on total RNA levels for each
331 gene in 0-2 hrs old embryos. For this, we used the results from the $Top3\beta^{26}$ null mutant (Adjp
332 <0.0002; log2-fold change <-1 and >1, respectively; **Supplementary Table S1**) and the
333 published results from an *FMR1* mutant (92). These analyses consider reads per gene and do
334 not discriminate between different RNA isoforms. Consistent with their physical interaction,

335 more than half of the genes affected in the *FMR1* mutant were also found affected in *Top3β*^{26}
336 (**Fig. 4B**). In both cases, only a few genes showed higher RNA levels in the mutant and the
337 overlap between the two elevated RNA datasets was very low. Lists of the genes identified in
338 the datasets of both mutants are presented in the supplements (**Supplementary Table S13**).

339 The role of Drosophila *Fmr1* in translation was also studied in quiescent oocytes using RNAi
340 treatment and analysis in ovaries (48). Comparing the list of their genes significantly repressed
341 in translation to the transcript isoforms less abundant in the extracts of *Top3β*^{26} mutants
342 (**Supplementary Table S4**) revealed several shared mRNAs (**Fig. 4C)**. Even though different
343 tissues had been used for the two experiments and different effects had been compared,
344 there is still an overlap between the two data sets. Again, *FMR1* and *Top3β* seem to act on
345 many of the same mRNAs, but they also seem involved in additional functions, independently
346 of each other. We also compared the effect of lack of Top3β on the RNASeq reads in 0-2 hrs
347 old embryos per gene with the effect the RNAi treatment against *FMR1* has on translational
348 repression (48) in the ovary. Using the data from **Supplementary Table S1** and the same
349 conditions as in **Fig. 4B** (Adjp <0.0002; log2-fold change <-1) we only found three hits in the
350 overlap with the same *FMR1* data (**Fig. 4D**), which had shown a good overlap with the list of
351 reduced transcript isoforms. Two reasons seem to explain the lower number in this overlap
352 compared to the ones in **B)** and **C)**. One, as mentioned by the authors, *FMR1* RNAi knockdown
353 did not generally reduce mRNA levels except for its own RNA (48). In contrast, the *FMR1*
354 mutant used in the study used for **B**) (92), reduced many RNA levels. Two, studying the effect
355 on transcript isoforms (as in **C)** is more sensitive to detecting level changes because the same
356 changes might be judged insignificant in the pool of different transcript isoforms of the same
357 gene.

358

359 **Top3β supports the expression and subcellular localization of its transcript targets**

360 The *Top3β*^{Y332F} and *Top3β*^{26} mutants have reduced or no function, but the mutations cause
361 neither lethality nor sterility. This is a common phenomenon observed with conserved genes
362 and proteins, which are still important for optimizing cellular physiology. In a lab setting, the
363 reduced function of these mutants can often be compensated for by other mechanisms.
364 However, by directly analyzing the cellular phenotypes of the mutants, one may observe
365 increased cellular stress and changes in physiology or anatomy that reveal the cellular
366 function of the normal gene. Such cellular stress and alteration often lead to signs of
367 premature aging, like a decline in neuromuscular performance and a shorter lifespan.

368 To evaluate the consequences of the interaction of Top3β with its RNA targets, we selected
369 *shot* (encoding a spectraplakin), *Dhc64C* (encoding the large subunit of the cytoplasmic dynein
370 motor), and *kst* (encoding the β_{Heavy}-spectrin) from the top list of RNAs covalently bound to
371 Top3β::eGFP for further analysis. Aside from exhibiting the typical RNA features of the top
372 targets, their homologs were also identified by the mammalian studies used for **Fig. 4A** (1)
373 and they are expressed in neurons, too (22)(23). In normal young embryos, *shot* mRNA
374 accumulates more strongly in the polar granules and the pole cells at the posterior end (**Fig.
375 5)**. In embryos that were maternally and zygotically mutant for *Top3β*, *shot* mRNA levels were
376 overall reduced. Additionally, the more intense, localized staining pattern in the posterior
377 pole region was lost in the null- and the enzymatic mutant *Top3β*^{Y332F}, but not in *Top3β*$^{\Delta RGG}$,
378 suggesting that the normal expression and localization of *shot* mRNA depends on *Top3β* and
379 particularly on its enzymatic activity. Analogous studies revealed that the anti-Shot antibody
380 signal was similarly weaker in *Top3β*^{26} and *Top3β*^{Y332F} embryos compared to the wild type

381 (**Fig. 5)**, suggesting that the reduced mRNA levels caused the reduced Shot protein expression.
382 These findings are consistent with *shot* mRNA being a primary target of Top3β and they
383 highlight the importance of the enzymatic activity of Top3β for the efficient expression and
384 localization of the encoded protein. *Top3β*$^{\Delta RGG}$ mutant embryos still show a reduction of the
385 Shot protein signal even though the RNA is still localized **(Fig. 4)**. This is consistent with the
386 role of Top3β in the translation of *shot* RNA. That Top3β is required for efficient translation
387 of mRNAs has already been demonstrated (74). The effects on the proteins encoded by two
388 more *Top3β* targets were similar. The cytoplasmic Dynein heavy chain (Dhc or Dhc64C)
389 protein accumulated more strongly at the posterior end of the wild-type embryo, in front of
390 the pole cells. This was neither detectable in the null mutant nor in *Top3β*^{Y332F} **(Fig. 5)**. The
391 Kst protein accumulated at the apical cortex in normal blastoderm embryos, but in the *Top3β*
392 null mutant and *Top3β*^{Y332F}, its signal was reduced throughout the embryo, including the
393 apical cortex. Protein signals for Dhc showed an intermediate strength in the *Top3β*$^{\Delta RGG}$
394 mutant embryos **(Fig. 5)**, indicating that the RGG box also affects their expression, albeit less
395 strongly than the catalytic activity. We conclude that *Top3β* facilitates gene expression and
396 particularly localized accumulation of proteins at sites distant from the nucleus.

397 Top3β normally localizes to the same area in blastoderm embryos as the different proteins
398 and mRNAs described here. In the Discussion section, we will detail how this seems to
399 contribute to an interesting gene expression mechanism. Note also that the wild-type protein
400 and Top3β^{Y332F} localize to the cytoplasm and the nuclei **(Fig. 5)**. In contrast, Top3β$^{\Delta RGG}$ is seen
401 above background levels only in the cytoplasm. This indicates that its RGG box is needed to
402 localize Top3β to the nucleus in blastoderm embryos and that the lack of the RGG box likely
403 reduces the nuclear functions of Top3β$^{\Delta RGG}$.

404

405 ***Top3β* supports neuronal structure and function in aging adults**

406 The negative geotaxis assay measures the activity of the nervous system and the muscles, and
407 the coordination between them. In this assay, all four *Top3β* genotypes showed similar
408 climbing abilities in young flies **(Fig. 6A).** Neuromuscular conditions sometimes become only
409 apparent at an older age because the young nervous system can compensate for some cellular
410 deficits. But such compensations can take their toll if they stress the cells. We, therefore,
411 tested for premature aging and age-related degeneration of the climbing ability. Indeed, as
412 seen in **Fig. 6A,** from week 6 on, the $Top3\beta^{Y332F}$ and $Top3\beta^{26}$ flies became slower, and their
413 climbing ability declined more than the wild-type one. The results suggest that Top3β plays a
414 role in aging and combating neurodegeneration in *Drosophila* motor neurons.

415 In aging flies with declining motor abilities and neurotransmission, fragmentation of synaptic
416 motor terminals becomes apparent (24). We studied the structure of the adult neuromuscular
417 junctions (NMJs) in the four genotypes during aging **(Fig. 6B)**. Particularly the young null
418 mutants contained more branched structures compared to the simpler branch structures in
419 the wild type. This might constitute a mechanism to compensate for less efficient synapse
420 function. Although to a lesser degree, young $Top3\beta^{Y332F}$ and $Top3\beta^{\Delta RGG}$ mutants also displayed
421 presynaptic overgrowth. Concomitant with the premature loss of locomotive ability around
422 week 6 **(Fig. 6A)**, denervation of the DLM (Dorsal Longitudinal Muscle) synapses became
423 evident. Particularly in the null mutants, but also in $Top3\beta^{Y332F}$, loss of synaptic integrity was
424 observed during aging in 1-2 months old adult flies **(Fig. 6B)**. The micrographs of these
425 mutants are likely an underestimate of the average effect of the mutation because $Top3\beta^{26}$
426 and $Top3\beta^{Y332F}$ flies live less long than $Top3\beta^{\Delta RGG}$ **(Fig. 6C)** and healthy flies, and only living

427 flies were selected for the NMJ preparation. The decline of the NMJ structure and function
428 was most likely more severe in the dead animals. In summary, it appears that the reduced
429 expression of many Top3β targets can initially be compensated in neurons for some time, but
430 over time they lead to premature aging of the nervous system and reduced neuromuscular
431 performance. It should be pointed out that a shorter life span has also been reported for
432 *Top3β*$^{-/-}$ mice (93).

433

434 ***Top3β* mutants enhance (G4C2)$_{49}$-induced neuronal toxicity in flies**

435 To gain deeper insights into the cellular significance of Top3β's catalytic activity toward one
436 specific RNA, we investigated its effect on the phenotype induced by GC-rich repeat RNA
437 sequences. For this, we used the repeat sequence (GGGGCC)$_{49}$ (also named G4C2)$_{49}$ that
438 induces neurotoxic effects in both humans and flies. In humans, the presence of 20-28 repeats
439 of this sequence was shown to be associated with neurodegenerative diseases such as
440 amyotrophic lateral sclerosis (ALS) and frontotemporal dementia (FTD) (25)(26)(27). Using a
441 GMR-GAL4 driver (28) to study the effect of this RNA on the adult eyes revealed that *Top3β*
442 mutants enhanced the neurotoxic effect of the (G4C2)$_{49}$ transcripts in the eyes of young flies
443 aged 1-2 days (**Fig. 7**). Of the *Top3β* mutants, *Top3β*^{26} and *Top3β*^{Y332F} exhibited the most
444 severe eye lesions with irregular ommatidial structures, and this was particularly evident from
445 the widespread cell death. Young *Top3β*$^{\Delta RGG}$ mutants displayed irregular ommatidia but
446 usually less cell death. After one month, the rough eye phenotype caused by the *Top3β*^{26} and
447 *Top3β*^{Y332F} mutants affected the entire eye, and widespread degeneration of ommatidial cells
448 was observed. These results show that the topoisomerase activity of Top3β counteracts the
449 toxic activity of the (G4C2)$_{49}$ transcripts in the Drosophila model for this disease **(Fig. 7)**.

450 **Discussion**

451 Top3β and its catalytic activity have a strong effect on the production of normal expression
452 levels of a considerable number of RNAs during embryonic development. The features of
453 these RNAs are the same as found in RNAs that are direct targets of the topoisomerase activity
454 of Top3β. This points to important cytoplasmic functions of the Top3β topoisomerase in
455 facilitating the translation of RNAs, translational control, and RNA localization. For instance,
456 longer ORFs increase the risk of stalling translation because structural problems of mRNAs
457 arise more frequently and prevent them from entering the ribosome. Top3β can rescue such
458 mRNAs (74). The top Top3β mRNA targets depended not only on *Top3β* for their normal
459 expression levels, but also for their localization within the cell (**Fig. 5**). Consistent with the
460 proposed role of Top3β in rescuing RNAs with structural problems, the absence of the RNA
461 topoisomerase activity does only reduce levels of affected RNAs and does not abolish them.
462 Additionally, we also found evidence for nuclear roles in splicing, alternative splicing, and
463 3'end formation. The protein interaction map (**Supplementary Fig. S5**) supports these
464 interpretations as well as its function in RNAi (49)**.**

465 RNA localization combined with translational control is a mechanism to provide local
466 expression of gene products. It is most important in large cells, but also for fine-tuning gene
467 expression in general. From our results, it seems likely that this lack of fine-tuning gene
468 expression of many genes, particularly the ones with the characteristics of *Top3β* targets and
469 *Top3β*-dependent transcripts, makes human *Top3β* mutations a risk factor for several
470 neurological diseases and cancers.

471

472 ***RNA targets of Top3β***

473 The Top3β interaction with splicing factors **(Supplementary Fig. S5; Table S9)** seems to
474 explain why Top3β's RNA targets often have a greater number of exons, longer introns, and
475 alternative transcripts **(Fig. 3)**. These parameters might require additional RNA
476 topoisomerase activity in the nucleus where Top3β presumably interacts with splice factors
477 and the pre-mRNA. As with many other splice factors, Top3β might remain associated with
478 the spliced mRNA in the cytoplasm (30)(31)(32)(33)(34). Nuclear translocation of Top3β
479 requires the RGG motif in the blastoderm embryo **(Fig. 5)**. Therefore, the *Top3β*$^{\Delta RGG}$ allele
480 should be a useful tool to analyze the nuclear localization and functions of Top3β. The RGG
481 motives can be arginine methylated in HeLa cells (89), where it was shown that this enhances
482 the interaction with TDRD3, the topoisomerase activity, and stress granule localization upon
483 Arsenite treatment. Whether and how this methylation affects the nuclear localization of
484 Top3β is, however, not clear yet.

485 The entanglement of long mRNAs and pre-mRNAs poses a considerable problem during
486 transport over extended distances. Some of these processes involve additional mRNA
487 packaging and unpackaging before the mRNAs can be activated for translation at the right
488 place and time (94). The resulting structural problems might then interfere with their
489 transport or, later, with their translation on ribosomes. The coding sequence (CDS) and
490 untranslated regions (UTRs) of mRNA molecules are important for regulating gene expression
491 at the level of RNA localization and translation. Particularly 3'UTRs affect not only the
492 translation in neurons but mostly also the localization to the places where these mRNAs will
493 be translated in response to extrinsic stimuli, such as neurotrophins, synaptic activation, and
494 regeneration after injury (36)(8)(37)(38) (94). Consistent with the proposed function of Top3β

495 in rescuing (pre-)mRNAs with such functions and characteristics, the *in vivo* targets of Top3β
496 displayed a strong bias for these characteristics (**Fig. 3; Supplementary Table S11**) and the
497 enzymatic activity of *Top3β* is particularly important for mRNAs that are generated from long
498 pre-mRNAs, for mRNAs with long 3'UTRs and CDSs (**Figs. 1B-D; Supplementary Table S7**).

499 ***Important targets of Top3β***

500 *Rop*, encodes a Sec-1-like protein involved in vesicle trafficking in neuronal synapses and non-
501 neuronal vesicle trafficking. In neuronal tissues, it regulates neurotransmitter secretion in a
502 dosage-dependent manner (6)(7). In *Rop* mutants, the release of neurotransmitters from the
503 pre-synapse area into the synaptic cleft fails to occur. In 7 neurological diseases with which
504 human *Top3β* had been associated and in Drosophila embryos, normal expression levels of
505 the *Rop* mRNA depend on *Top3β* (**Fig. 2C**; **Supplementary Table S7**). *Rop* is likely a rewarding
506 gene to investigate these neurological diseases. It was the only gene that was present in all 8
507 datasets and the *Rop* mRNA was a significant direct target of Top3β **(Supplementary Table**
508 **S10).**

509 *shot* was identified in most experimental datasets analyzed. *shot* mRNA is a top Top3β target
510 (**Supplementary Tables S10, S11**), in Drosophila and HeLa cells and also as an FMRP target in
511 mouse brains (**Fig. 4A**; (1)(74)). In young Drosophila embryos, normal levels of a specific *shot*
512 mRNA isoform also depend on *Top3β* and its enzymatic activity (**Supplementary Table S5**),
513 and *shot* mRNAs and protein levels appeared reduced and less localized in embryos **(Fig. 5).**
514 *shot* encodes a spectraplakin family member, a large cytoskeletal linker molecule that binds
515 actin and microtubules and participates in axon growth and neuromuscular junction
516 maintenance and growth control (39),(40),(41),(42). Drosophila *shot* has additional roles in
517 many other tissues and cell types, and it consists of 45 exons producing 22 transcript isoforms,

518 as opposed to 2 isoforms per gene, which is average for *Drosophila*. The reduced *shot* mRNA
519 and protein levels and localization might reflect roles of Top3β in splicing *shot* pre-mRNAs,
520 localizing *shot* mRNA, resolving RNA entanglements, and facilitating *shot* mRNA translation.

521 Localization of mRNAs combined with translational control is a mechanism that is particularly
522 important in large cells (like oocytes and young embryos) and cells with large extensions (like
523 neurons) (94). Many of the identified mRNAs function in such cells and have important roles
524 in neurons because they encode large cytoskeletal and cortical elements (e.g., *kst*, *α-spec*,
525 *shot, mgl*) or regulators of NMJ growth (e.g., *Prosap*). Along with α-Spec, Kst (β_H-Spectrin)
526 crosslinks F-actin and acts as a molecular scaffold when recruited to the apical membrane of
527 epithelial cells (43)(44)(Fig. 5). Because cortical localization seems to be one of the processes
528 that is most dependent on the RNA topoisomerase activity, it is relevant that Top3β
529 accumulates preferentially at the apical cortex of embryos, too. Higher Top3β activity in this
530 location is expected to contribute to the apical translatability of mRNAs – for instance by
531 rescuing entangled mRNAs -, thereby expressing the encoded protein apically at higher levels.
532 Therefore, the subcellular localization of Top3β activity seems to serve as an additional tool
533 to target gene expression efficiently to specific cellular locations. Such a mechanism can even
534 produce protein localization if the mRNA is expressed uniformly.

535 ***Top3β environment and relevance***

536 The enrichment of neuronal-, stress-, and other ribonucleoprotein (RNP) forming granules,
537 was a clear result of the analysis of the Top3β interactors (**Supplementary Fig. S5;**
538 **Supplementary Table S9**). In the case of the neuronal RNP granules, they concentrate specific
539 sets of mRNAs and regulatory proteins in the same location, promoting their common long-
540 distance transport to axons or dendrites (20)(21). They also have a dual function in regulating

541 the translation of associated mRNAs (47). As a component of neuronal RNPs, Me31B mediates
542 the transport and controls the translation of neuronal RNAs, including the translational
543 repression of synaptic transcripts (26). We found Me31B highly enriched with Top3β and this
544 interaction depended on the RGG box, suggesting that the RGG box can link Top3β to
545 neuronal RNPs. It will be interesting to find out whether this localization is also controlled by
546 Arg-methylation of these motives as reported for stress granule localization of Top3β (89).

547 The lack of RNA topoisomerase activity can interfere with the expression of many different
548 genes involved in a variety of different pathways. The resulting suboptimal functioning of
549 different cellular mechanisms is likely to interfere with cellular physiology, making it less
550 efficient and producing cellular stress. Further research needs to test which of the individual
551 pathways suggested by our work causes a physiological problem in the human conditions
552 involving *Top3β*. Serious neurological health issues often arise when several pathways are not
553 functioning properly anymore, making it difficult to pinpoint a single primary cause. Our work
554 revealed that reduced activity of Top3β affects several of the pathways that rely on mRNAs
555 that are Top3β targets. The combination of defects in different physiological pathways is likely
556 to impact the outcome of the various neurodevelopmental and cognitive disorders and
557 cancers with altered *Top3β* function.

558

559 ## Material and Methods

560 ### Fly stocks and maintenance

561 The *white* (*w)* strain was used as a wild-type control as this was the genetic background of the
562 mutants used in this study. The mutant fly stocks *Top3β*^{Y332F} and *Top3β*$^{\Delta RGG}$ were established
563 as described below. *Top3β*^{26} was obtained from Lee and colleagues (49) and described by Wu
564 et al (50). The fly stocks were grown and maintained on a regular corn medium (ingredients:
565 corn, yeast powder, sucrose syrup, agar, potassium sodium tartrate tetrahydrate, water,
566 nipagin, and propionic acid) supplied with brewer's yeast for the experiments. All *Drosophila*
567 *melanogaster* fly stocks were stored at 18°C in glass or plastic vials with day/night (12 h/12 h)
568 light cycles. All experiments were performed at 25°C. $(G4C2)_{49}$ flies (Stock #84727; (28))
569 express 49 pure 5'GGGGCC3' repeats under the control of UAS. These repeats are neurotoxic
570 and model the G4C2 repeats seen in human *C9orf72* that are associated with Amyotrophic
571 Lateral Sclerosis and Frontotemporal Dementia.

572 ### Generation of *Top3β* alleles

573 Genomic sequences were scanned for suitable sgRNA target sites with the JBrowse from
574 FlyBase and appropriate sgRNA sequences were chosen based on (a) their distance from the
575 tagging site, and (b) the absence of potential off-target sites on the same chromosome as the
576 target site (51). To mutate the endogenous *Top3β*, a sgRNA was designed, which hybridized
577 in the vicinity of the Y332 codon of *Top3β* and induced the Cas9 nuclease to perform a double-
578 strand break. Complementary oligodeoxynucleotides with suitable overhangs
579 (**Supplementary Table S12**) were annealed and cloned into the pCFD5 vector, which is used
580 to express the sgRNA (52). The Cas9 fly stock was obtained from the Bloomington Stock
581 Center (#79004). ssDNA was designed for the mutation changing the Tyr (Y) to a Phe (F) codon

582 and injected into the progeny produced by Cas9- and sgRNA-expressing flies. The single-
583 strand oligodeoxynucleotide with the flanking arms precisely matching the endogenous
584 sequences changes the sequence at the mutation site by serving as a template
585 (**Supplementary Table S12**) for the homologous recombination DNA repair at the double-
586 strand break. The same strategy was used to delete the endogenous RGG region in *Top3β*
587 (ΔRGG) using the appropriate gRNA and ssDNA templates. Stocks were established from
588 individual mutants and genomic sequencing confirmed the precise mutation events in the
589 initial mutant fly and the final stock. Stocks were deposited in the Bloomington Drosophila
590 Stock Center (presently as #99728 and #99728). Both point mutants produce normal RNA
591 levels (**Supplementary Table S1-3**) and produce stable proteins **(Fig. 5)** – although Top3$\beta^{\Delta RGG}$
592 was absent from the syncytial nuclei. That the point mutations of these two mutants do not
593 affect protein levels was also shown by qMS analysis of the tagged versions of these proteins
594 which gaave very similar results **(Supplementary Table S9**).

595 **RNA sequencing**

596 RNA was isolated using 1 ml of TRIzol® Reagent per 50-100 mg of tissue samples (0-2 hours
597 embryos). The samples were homogenized at room temperature. RNA extraction was done
598 according to the Trizol protocol. The University of Bern's Next Generation Sequencing
599 Platform conducted quality control assessments, library generation, sequencing runs, and
600 sequencing quality control steps. The purified total RNA was assessed for quantity and quality
601 using a Thermo Fisher Scientific Qubit 4.0 fluorometer with the Qubit RNA BR or HS Assay Kit
602 (Thermo Fisher Scientific, Q10211 or Q32855, respectively) and an Agilent Advanced
603 Analytical Fragment Analyzer System using a Fragment Analyzer RNA Kit (Agilent, DNF-471),
604 respectively. rRNA depletion and construction of sequencing libraries were performed

605 according to Lexogen's guidelines using a CORALL Total RNA-Seq Library Prep Kit with UDI
606 12nt Set A1 (Lexogen, 117.96). The libraries were paired-end sequenced using either shared
607 Illumina NovaSeq 6000 SP, S1, or S2 Reagent Kits (200 cycles; Illumina, 200240719, 2002831,
608 or 20028315) on an Illumina NovaSeq 6000 instrument. The quality of the sequencing runs
609 was assessed using the Illumina Sequencing Analysis Viewer (Illumina version 2.4.7), and all
610 base call files were demultiplexed and converted into FASTQ files using Illumina bcl2fastq
611 conversion software v2.20.

612 The quality and quantity of reads generated from RNA-seq were evaluated. Most of the
613 reads were from mature transcripts without introns, but we mapped them to the reference
614 genome that includes introns using an alignment tool like Hisat2 that can handle large gaps.
615 This required information on where each gene is located in the genome, available for
616 example from Ensemble (53). The number of reads mapping to each gene was counted
617 using the FeatureCounts tool. This resulted in a table of read counts for each sample and
618 gene. The bulk RNA seq data has been posted on NCBI-GEO
619 (https://www.ncbi.nlm.nih.gov/geo/query/acc.cgi?acc=GSE249429).

620 To test for differential expression between two experimental groups containing three
621 biological replicates each, we used the DESeq2 tool. The analysis included the following
622 steps: 1. Normalization to correct for differences in the total number of reads between
623 samples. 2. Variance estimation between replicates to account for the limited number of
624 replicates in RNA-seq experiments (DESeq2 incorporates information from other genes with
625 similar overall expression levels into the estimation). 3. Log-fold change (LFC) adjustment
626 based on evidence strength which was estimated by the LFC. If it is weak (e.g., because the
627 gene is expressed at low levels, the variance between replicates is high, or there are few
628 replicates), the LFC shrinks toward zero. 4. Calculation of a test statistic and comparison to

629 the normal distribution to obtain a p-value. 5. Multiple test corrections using the Benjamini-
630 Hochberg procedure to consider only potentially detectable, differentially expressed genes.
631 DESeq2 applies a false discovery rate correction based on the Benjamini-Hochberg
632 procedure. However, the multiple-test correction considers only genes that could
633 potentially be detected as differentially expressed. Only these genes will have an adjusted p-
634 value. The mean read count across all samples is used to decide if a gene should be included
635 or not. Mapping of the sequence reads to specific isoforms was performed with the Salmon
636 method (91). The Venn diagrams in Fig. 1A were produced with the online tool of the Ghent
637 University (https://bioinformatics.psb.ugent.be/webtools/Venn/).

638 **Extracting transcript features**

639 The information about exon length, exon count, 3´UTR length, gene name, gene length, 5´UTR
640 length, mRNA length, and CDS length was extracted from the gtf file of dmel-all-filtered-
641 r6.42.gff using a custom python script.

642 **Generation of the *Top3β::eGFP* cDNA clone for GAL4>UAS expression**

643 For the *Top3β::eGFP* construct, the *Top3β* cDNA clone LD10035 was amplified. Enhanced GFP
644 (EGFP) was PCR amplified from a plasmid (pEGFP–C3). PCR amplified fragments were run on
645 an agarose gel and purified using the Wizard SV kit (Promega). The sequences were cloned
646 into the pUASz1.0 vector (54) with the *eGFP* ORF at the C-terminal end of the *Top3β* ORF using
647 a ligation kit (NEB). The UASz vector allows one to induce the constructs in any tissue,
648 including the somatic tissue, the germline, and the CNS (54). Plasmids were sequenced to
649 confirm the integrity of the construct and purified with a PureYield kit (Promega) for injection.
650 Transgenic stocks were established with the attP landing platform 86F from the Bloomington
651 Stock Center (#24749) and also deposited in the Stock Center (#99726).

652 To generate an enzymatically dead enzyme, a Phe codon substituted the codon for the Tyr
653 responsible for crosslinking the enzyme with the nucleic acid in the *UASz-Top3β::eGFP* vector
654 to give rise to *UASz-Top3β*^{Y332F}*::eGFP*. Similarly, to figure out the role of the RGG box, we
655 deleted in the *UASz-Top3β::eGFP* vector the sequence coding for this box, giving rise to *UASz-*
656 *Top3β*$^{\Delta RGG}$*::eGFP*. At the site of the desired mutation, oligonucleotide primers with the
657 desired mutation were used to amplify the mutant double-stranded DNA plasmid
658 (**Supplementary Table S12)**. A protocol based on two different PCR amplifications was used
659 for this. First, two elongation reactions were carried out, with one of the two primers each.
660 In the second reaction, the two initial elongation reactions were mixed and an additional PCR
661 reaction was carried out. The eGFP fusion constructs were transformed into *Drosophila* using
662 the attP-86F landing platform. They are also available from the Bloomington Stock Center
663 (#99725 and #99727). mat-tub-GAL4 (#7062) was used to drive the expression in the older
664 female germline. The wild-type and the mutant eGFP fusions were expressed at similar levels
665 as determined by qMS analysis **(Supplementary Table S9**). UASz-eGFP transgenic flies,
666 obtained from the Bloomington stock center, were used as negative controls.

667 **Sample preparation for mass spectrometry**

668 Drosophila Top3β::eGFP was purified using the GFP tag and a mouse anti-eGFP antibody as
669 described previously (55). Protein G magnetic beads were washed 3x with PBS and incubated
670 for 2 hours with an anti-GFP antibody. After this, they were washed 3x with 1 ml 1x PBS and
671 one more time with 1 ml homogenization buffer (25 mM Hepes PH 7.4; 150 mM NaCl; 0.5
672 mM EDTA PH 8.0, 1 mM DTT, protease inhibitors). To prepare the extracts, 1 ml
673 homogenization buffer was added to 1 gr of the samples (dechorionated embryos 0-2 hours)
674 in the glass homogenizer. The samples were homogenized and transferred into the tube.

675 Homogenized samples were centrifuged at 16,000 g (RCF), 4°C for 40 min. The interphase was
676 transferred into a fresh Eppendorf tube, centrifuged again at 16,000 g, 4°C for 40 min, and
677 transferred into a fresh tube. Beads were then incubated with the extracts for 6 hours at 4°C
678 on a wheel and the extracts were subsequently removed from the beads. The beads were
679 washed once with 1 ml homogenization buffer and then several times with wash buffer (25
680 mM Hepes PH 7.4; 150 mM NaCl; 0.5 mM EDTA PH 8.0; 1 mM DTT; protease inhibitors). The
681 wash buffer was removed, and the beads were sent for mass spectrometry.

682 **Mass spectrometry**

683 Mass spectrometry analysis was done by the Proteomics and Mass Spectrometry Core Facility
684 of the University of Bern, and the data are available in **Supplementary Table S9**. Proteins in
685 the affinity pull-down were re-suspended in 8M Urea / 50 mM Tris-HCl pH8, reduced for 30
686 min at 37°C with 0.1M DTT / 100 mM Tris-HCl pH8, alkylated for 30 min at 37°C in the dark
687 with IAA 0.5M / 100 mM Tris-HCl pH8, dilute with 4 volumes of 20 mM Tris-HCl pH8 / 2 mM
688 CaCl2 before overnight digestion at room temperature with 100 ng sequencing grade trypsin
689 (Promega). Samples were centrifuged, and a magnet holder trapped the magnetic beads to
690 extract the peptides in the supernatant. The digests were analyzed by liquid chromatography
691 (LC)-MS/MS (PROXEON coupled to a QExactive mass spectrometer, ThermoFisher Scientific)
692 with three injections of 5 µl digests. Peptides were trapped on a µPrecolumn C18 PepMap100
693 (5 µm, 100 Å, 300 µm×5 mm, ThermoFisher Scientific, Reinach, Switzerland) and separated
694 by backflush on a C18 column (5 µm, 100 Å, 75 µm×15 cm, C18) by applying a 60 min gradient
695 of 5% acetonitrile to 40% in water, 0.1% formic acid, at a flow rate of 350 ml/min. The Full
696 Scan method was set with a resolution at 70,000 with an automatic gain control (AGC) target
697 of 1E06 and a maximum ion injection time of 50 ms. The data-dependent method for

698 precursor ion fragmentation was applied with the following settings: resolution 17,500, AGC
699 of 1E05, maximum ion time of 110 milliseconds, mass window 2 m/z, collision energy 27,
700 underfill ratio 1%, charge exclusion of unassigned and 1+ ions, and peptide match preferred,
701 respectively.

702 The data were then processed with the software MaxQuant (56) version 1.6.14.0 against the
703 UniProtKB(57) Drosophila 7228 database (release 2021_02) containing canonical and isoform
704 entries, to which common contaminants were added. The following parameters were set:
705 digestion by strict trypsin (maximum three missed cleavages), first search peptide tolerance
706 of 15 ppm, MS/MS match tolerance of 20 ppm, PSM and protein FDR set to 0.01 and a
707 minimum of 2 peptides requested per group. Carbamidomethylation on cysteine was selected
708 as a fixed modification; the following variable modifications were allowed: methionine
709 oxidation, deamidation of asparagines and glutamines, and protein N-terminal acetylation; a
710 maximum of 3 modifications per peptide was allowed. Match between runs was turned on
711 (match time windows 0.7 min) but only allowed within replicates of the same kind.

712 Peptides were normalized by variance stabilization (58), imputed and combined to form Top3
713 (59) intensities, and considered alongside MaxQuant's Label-Free Quantification (LFQ) values.
714 Missing peptides, respectively LFQ intensities, were imputed by drawing values from a
715 Gaussian distribution of width 0.3 centered at the sample distribution mean minus 2.5x the
716 sample standard deviation, provided there were at most 1 non zero value in the group;
717 otherwise, the Maximum Likelihood Estimation (60) was used. Differential expression was
718 performed by applying the empirical Bayes test (61) between groups; significance testing was
719 performed as described (62).

720 **RNA immunoprecipitation**

721 Protein G magnetic beads were washed 2-3x with 1ml blocking buffer (20 mM Hepes, 150
722 mM KCl, 20% Glycerol, 0.5 % Tween, BSA (Biolabs), Heparin 0.2 mg/ml, SDS 0.1%, 1/2 pill EDTA
723 free protease inhibitors). Beads were blocked with a blocking buffer for 2-3 hours at room
724 temperature. Anti-GFP antibody was added to the beads and rotated for 1-2 hours. Beads
725 were washed 3x with non-hypotonic lysis buffer (20 mM Hepes, 1 mM EDTA, 150 mM KCL, 1
726 mM DTT, 0.5% Tween, 20% glycerol, SDS 0.1%, 1/2 pill EDTA free protease inhibitors).

727 Dechorionated embryos were 0-2 hours old. 1g of the embryos were homogenized in 2 ml
728 hypotonic lysis buffer (20 mM Hepes, 10 mM KCL, 1 mM EDTA, 1 mM DTT, 0.5% Tween, SDS
729 0.1%, 1/2 pill EDTA free protease inhibitors, and RNase inhibitor (Biolabs, 40,000U/ml)). 600
730 μl of extract, 323 μl of Adjusting buffer (57% Glycerol 100%, 0.4M KCl, 1 mM EDTA, 1 mM
731 DTT, 20 mM Hepes, SDS 0.1%), and 2 μl of RNase-free DNase I (20 μ/ml, Roche) were added
732 to the washed antibody beads and were precipitated ON rotating at 4°C. Samples were
733 washed 8x with 1 ml high salt wash buffer (20 mM Hepes, 1 mM EDTA, 200 mM KCl, 1 mM
734 DTT, 0.5% Tween, 20% Glycerol, SDS 0.1%, 1/2 pill EDTA free protease inhibitors, and RNase
735 inhibitor (Biolabs, 40,000U/ml)). On the last wash, 100 μl of the samples were taken before
736 centrifugation. 100 μl of proteinase K buffer, 1.5 μl proteinase K (20 mg/ml Roche), and RNase
737 inhibitors were added to each tube and were incubated for 30 minutes at 55°C. 1 ml Trizol
738 reagent was added to each tube, and RNA was extracted according to the Trizol protocol
739 (TRIzol™ Reagent, Invitrogen™, Catalog number: 15596026).

740 The Next Generation Sequencing Platform, University of Bern, conducted quality control
741 assessments, library generation, sequencing runs, and sequencing quality control steps. The
742 quantity and quality of the purified total RNA were assessed using a Thermo Fisher Scientific
743 Qubit 4.0 fluorometer with the Qubit RNA BR or HS Assay Kit (Thermo Fisher Scientific,

744 Q10211 or Q32855, respectively) and an Advanced Analytical Fragment Analyzer System using
745 a Fragment Analyzer RNA Kit (Agilent, DNF-471), respectively. Sequencing libraries were made
746 using a CORALL Total RNA-Seq Library Prep Kit, Version 1 with UDI 12nt Set A1 (Lexogen,
747 117.96) according to Lexogen's guidelines for this kit. For the library preparation, purified RNA
748 was neither depleted for rRNA nor selected for poly(A+) RNA but used directly for reverse
749 transcription with random primers. Pooled cDNA libraries were paired-end sequenced using
750 either shared Illumina NovaSeq 6000 SP, S1, or S2 Reagent Kits (200 cycles; Illumina,
751 200240719, 2002831, or 20028315) on an Illumina NovaSeq 6000 instrument. The quality of
752 the sequencing run was assessed using Illumina Sequencing Analysis Viewer (Illumina version
753 2.4.7) and all base call files were demultiplexed and converted into FASTQ files using Illumina
754 bcl2fastq conversion software v2.20.

755 The quality of the RNA-seq reads was assessed using fastqc v0.11.9 (63) and RSeQC v4.0.0
756 (64). Unique molecular identifiers (UMI) were extracted with umi-tools v1.1.2 (65), and
757 adapters were trimmed with cutadapt v3.4.1 (66) according to manufacturer instructions. The
758 reads were aligned to the Drosophila reference genome (BDGP6.32) using hisat2 v2.2.1 (67).
759 FeatureCounts v2.0.1 (68) was used to count the number of reads overlapping with each gene
760 as specified in release 103 of the Ensembl genome annotation. The Bioconductor package
761 DESeq2 v1.36.0 (69) was used to test for differential gene expression between the
762 experimental groups. To generate the log2 fold change versus transcript length plots, the
763 estimated log2 fold change per gene was plotted against the most extended transcript length
764 per gene with R v4.2.1 (70). We used the log2 fold change>=1 and the adjusted p-value (adjp-
765 value) <0.05 of enrichment over control for further analysis.

766 **Immunolocalization and FISH**

767 For the immunostaining of adult Dorsal Longitudinal Muscles (DLMs), thoraces of 0-3 days old
768 and 2 months old adult wild-type, *Top3β*^{Y332F}, *Top3β*$^{\Delta RGG}$, and *Top3β*^{26} flies were separated
769 from the rest of the body in 1x PBS. The thoraces were fixed in PFA (32% formaldehyde diluted
770 to 4% with 1x PBS) for 30 min at room temperature and then washed 3x with PBS. All 1x PBS
771 was removed from the tubes using a Pasteur pipette. The tubes were submerged into a liquid
772 nitrogen flask for 10 seconds using cryogenic tweezers. Then, 300 µL of ice-cold 1x PBS was
773 added to the samples. The thoraxes were cut into two hemithoraxes, transferred into 1x PBS
774 (24), and blocked in 1x PBS with 0.1% normal goat serum and 0.2% Triton X-100 at pH 7.4 for
775 at least one h at 4°C. Mouse anti-HRP or anti-Brp (nc82; 1:125 dilution) from Developmental
776 Studies Hybridoma Bank were used to stain motor neurons. Primary antibodies were removed
777 on the following day and the tissue was washed four times with PBST for 5 min each on a
778 rotator. For the secondary antibody staining, goat anti-mouse A647 (1.5 mg/ml, diluted 1:200
779 dilution; Jackson ImmunoResearch Laboratories Inc.) was added to the samples, which were
780 then kept at room temperature for 2 hours in a dark box on the rotator. After the 2 h
781 incubation, the secondary stain was washed out 4 times for 5 min with PBST. Then, the
782 samples were mounted on a slide (24).

783 Embryonic RNA in situ hybridizations (FISH) and antibody staining techniques, respectively,
784 were carried out as described previously in references (81) and (82), respectively. Anti-βH-
785 Spectrin/Kst antibody (no. 243 used at 1:500–1:600) was obtained from (83), anti-Shot
786 (mAbRod1) and anti-Dhc (2C11-2) antibodies were obtained from the Developmental Studies
787 Hybridoma Bank (https://dshb.biology.uiowa.edu).

788

789 **Negative geotaxis (climbing) assays**

790 Wild-type flies and the three *Top3β* mutant strains were reared on fresh food and allowed to
791 hatch at 25° C. For each genotype, all 0-3-day-old adult male flies were collected. Ten young
792 adult male flies, each, were anesthetized and placed in 4 separate graduated flat-bottom glass
793 cylinders. After 1 hour of recovery from CO_2 exposure, flies were gently tapped 4x to the
794 bottom of the cylinder to startle them repeatedly with constant force to displace the flies to
795 the bottom surface. The flies were then allowed to climb the wall until they reached the top
796 of the column. The climbing procedure was video recorded using an iPhone 11 Pro. These
797 assays were repeated every week over 7 weeks on the same weekday. Three fly batches, each,
798 provided the material for the triplicates which were performed within 5-minute intervals.
799 After the three trials, each batch of 10 flies was transferred into glass vials and kept at 25° C.
800 Before the experiment, every single batch was inspected to ensure that all 40 flies could be
801 video-tracked when they started to climb after the tapping. To calculate each climbing index
802 (CI), flies that remained at the bottom were counted as in zone 0. The formula used to
803 calculate the CI is CI = (0 x n0 + 1 x n1 + 2 x n2 + 3 x n3 + 4 x n4 + 5 x n5) / nTotal, where nTotal
804 is the total number of flies and nx is the number of flies that reached zone x.

805 **Statistics**

806 All statistical analyses were performed using GraphPad Prism 8. For the negative geotaxis
807 assays, the means, standard error of the means, and p-values were obtained by two-way
808 ANOVA with Tukey's multiple comparison test.

809

810

Acknowledgments

Our thanks go to P. Nicholson and the members of the University of Bern NGS platform for sequencing the many RNA samples and to the IBU group of R. Bruggmann, particularly, S. Oberhänsli, G. van Geest, and R. Dörig for their important support during the analyses of the sequencing data and for providing the proof of the correct mutations for the reviewers. We thank the University of Bern (Switzerland) Mass Spectrometry Center (PMSCF) members S. Braga Lagache and N. Buchs for performing the MS experiments and M. Heller and A-C. Uldry for the data analysis. We wish to acknowledge all our group members who gave their time and expertise to provide critical input and technical support. Special thanks go to P. Vazquez, R. Dörig, and D. Beuchle. We highly appreciate the continuous support from friends and colleagues in the Drosophila community for sharing their results, fly stocks, and antibodies. For this work, too, FlyBase provided invaluable support, the Developmental Studies Hybridoma Bank provided antibodies, and the Bloomington Drosophila Stock Center (NIH P40OD018537) fly stocks.

Funding

This work was supported by the Swiss National Science Foundation project grants 31003A_173188 and 310030_205075 and by the Equipment grant 316030_150824 to BS. Support came also from the University of Bern to BS. The funders had no role in study design, data collection, and interpretation, or the decision to submit the work for publication.

832 **References**

833 1. Xu D, Shen W, Guo R, Xue Y, Peng W, Sima J, et al. Top3β is an RNA topoisomerase
834 that works with fragile X syndrome protein to promote synapse formation. Nat
835 Neurosci. 2013;16(9):1238.

836 2. Ahmad M, Shen W, Li W, Xue Y, Zou S, Xu D, et al. Topoisomerase 3β is the major
837 topoisomerase for mRNAs and linked to neurodevelopment and mental dysfunction.
838 Nucleic Acids Res. 2017;45(5):2704–13.

839 3. Kaufman CS, Genovese A, Butler MG. Deletion of TOP3B is associated with cognitive
840 impairment and facial dysmorphism. Cytogenet Genome Res. 2016;150(2):106–11.

841 4. Dekker NH, Rybenkov V V, Duguet M, Crisona NJ, Cozzarelli NR, Bensimon D, et al.
842 The mechanism of type IA topoisomerases. Proc Natl Acad Sci. 2002;99(19):12126–
843 31.

844 5. Piñero J, Saüch J, Sanz F, Furlong LI. The DisGeNET cytoscape app: Exploring and
845 visualizing disease genomics data. Comput Struct Biotechnol J. 2021;19:2960–7.

846 6. Wu MN, Littleton JT, Bhat MA, Prokop A, Bellen HJ. ROP, the Drosophila Sec1
847 homolog, interacts with syntaxin and regulates neurotransmitter release in a dosage-
848 dependent manner. EMBO J. 1998;17(1):127–39.

849 7. Schulze KL, Littleton JT, Salzberg A, Halachmi N, Stern M, Lev Z, et al. Rop, a
850 Drosophila homolog of yeast Sec1 and vertebrate n-Sect/Munc-18 proteins, is a
851 negative regulator of neurotransmitter release in vivo. Neuron. 1994;13(5):1099–108.

852 8. Zhang W, Liu HT. MAPK signal pathways in the regulation of cell proliferation in
853 mammalian cells. Cell Res. 2002;12(1):9–18.

854 9. Huang R, Quan Y, Chen J, Wang T, Xu M, Ye M, et al. Osteopontin promotes cell
855 migration and invasion, and inhibits apoptosis and autophagy in colorectal cancer by
856 activating the p38 MAPK signaling pathway. Cell Physiol Biochem. 2017;41(5):1851–
857 64.

858 10. Baker NM, Rajan R, Mondragón A. Structural studies of type I topoisomerases.
859 Nucleic Acids Res. 2009;37(3):693–701.

860 11. Pommier Y, Sun Y, Shar-yin NH, Nitiss JL. Roles of eukaryotic topoisomerases in

861 transcription, replication and genomic stability. Nat Rev Mol cell Biol.
862 2016;17(11):703.

863 12. Nostramo R, Xing S, Zhang B, Herman PK. Insights into the role of P-bodies and stress
864 granules in protein quality control. Genetics. 2019;213(1):251–65.

865 13. Siaw GE-L, Liu I-F, Lin P-Y, Been MD, Hsieh T. DNA and RNA topoisomerase activities
866 of Top3β are promoted by mediator protein Tudor domain-containing protein 3. Proc
867 Natl Acad Sci. 2016;113(38):E5544–51.

868 14. Nakamura A, Amikura R, Hanyu K, Kobayashi S. Me31B silences translation of oocyte-
869 localizing RNAs through the formation of cytoplasmic RNP complex during Drosophila
870 oogenesis. 2001;

871 15. Wilhelm JE, Buszczak M, Sayles S. Efficient protein trafficking requires trailer hitch, a
872 component of a ribonucleoprotein complex localized to the ER in Drosophila. Dev
873 Cell. 2005;9(5):675–85.

874 16. Barbee SA, Estes PS, Cziko A-M, Hillebrand J, Luedeman RA, Coller JM, et al. Staufen-
875 and FMRP-containing neuronal RNPs are structurally and functionally related to
876 somatic P bodies. Neuron. 2006;52(6):997–1009.

877 17. Liu J, Carmell MA, Rivas F V, Marsden CG, Thomson JM, Song J-J, et al. Argonaute2 is
878 the catalytic engine of mammalian RNAi. Science (80-). 2004;305(5689):1437–41.

879 18. Wang M, Ly M, Lugowski A, Laver JD, Lipshitz HD, Smibert CA, et al. ME31B globally
880 represses maternal mRNAs by two distinct mechanisms during the Drosophila
881 maternal-to-zygotic transition. Elife. 2017;6:e27891.

882 19. Lee J, Yoo E, Lee H, Park K, Hur J-H, Lim C. LSM12 and ME31B/DDX6 define distinct
883 modes of posttranscriptional regulation by ATAXIN-2 protein complex in Drosophila
884 circadian pacemaker neurons. Mol Cell. 2017;66(1):129–40.

885 20. Hillebrand J, Barbee SA, Ramaswami M. P-body components, microRNA regulation,
886 and synaptic plasticity. ScientificWorldJournal. 2007;7:178–90.

887 21. Ruscica V, Bawankar P, Peter D, Helms S, Igreja C, Izaurralde E. Direct role for the
888 Drosophila GIGYF protein in 4EHP-mediated mRNA repression. Nucleic Acids Res.
889 2019;47(13):7035–48.

890 22. Lee S, Kolodziej PA. Short Stop provides an essential link between F-actin and
891 microtubules during axon extension. 2002;

892 23. Liu Z, Steward R, Luo L. Drosophila Lis1 is required for neuroblast proliferation,
893 dendritic elaboration and axonal transport. Nat Cell Biol. 2000;2(11):776–83.

894 24. Sidisky JM, Babcock DT. Visualizing synaptic degeneration in adult Drosophila in
895 association with neurodegeneration. JoVE (Journal Vis Exp. 2020;(159):e61363.

896 25. DeJesus-Hernandez M, Mackenzie IR, Boeve BF, Boxer AL, Baker M, Rutherford NJ, et
897 al. Expanded GGGGCC hexanucleotide repeat in noncoding region of C9ORF72 causes
898 chromosome 9p-linked FTD and ALS. Neuron. 2011;72(2):245–56.

899 26. Renton AE, Majounie E, Waite A, Simón-Sánchez J, Rollinson S, Gibbs JR, et al. A
900 hexanucleotide repeat expansion in C9ORF72 is the cause of chromosome 9p21-
901 linked ALS-FTD. Neuron. 2011;72(2):257–68.

902 27. Vatsavayai SC, Nana AL, Yokoyama JS, Seeley WW. C9orf72-FTD/ALS pathogenesis:
903 evidence from human neuropathological studies. Acta Neuropathol. 2019;137:1–26.

904 28. Goodman LD, Prudencio M, Kramer NJ, Martinez-Ramirez LF, Srinivasan AR, Lan M, et
905 al. Toxic expanded GGGGCC repeat transcription is mediated by the PAF1 complex in
906 C9orf72-associated FTD. Nat Neurosci. 2019;22(6):863–74.

907 29. Mignone F, Gissi C, Liuni S, Pesole G. Untranslated regions of mRNAs. Genome Biol.
908 2002;3:1–10.

909 30. Ast G. How did alternative splicing evolve? Nat Rev Genet. 2004;5(10):773–82.

910 31. Black DL. Protein diversity from alternative splicing: a challenge for bioinformatics
911 and post-genome biology. Cell. 2000;103(3):367–70.

912 32. Budagyan B, Loraine A. Gene length and alternative transcription in fruit fly. In:
913 Proceedings 2004 IEEE Computational Systems Bioinformatics Conference, 2004 CSB
914 2004. IEEE; 2004. p. 515–6.

915 33. McGuire AM, Pearson MD, Neafsey DE, Galagan JE. Cross-kingdom patterns of
916 alternative splicing and splice recognition. Genome Biol. 2008;9(3):1–19.

917 34. Fox-Walsh KL, Dou Y, Lam BJ, Hung S, Baldi PF, Hertel KJ. The architecture of pre-

918 mRNAs affects mechanisms of splice-site pairing. Proc Natl Acad Sci.
919 2005;102(45):16176–81.

920 35. Liang J, Wen J, Huang Z, Chen X, Zhang B, Chu L. Small nucleolar RNAs: insight into
921 their function in cancer. Front Oncol. 2019;9:587.

922 36. Han K, Gennarino VA, Lee Y, Pang K, Hashimoto-Torii K, Choufani S, et al. Human-
923 specific regulation of MeCP2 levels in fetal brains by microRNA miR-483-5p. Genes
924 Dev. 2013;27(5):485–90.

925 37. Tushev G, Glock C, Heumüller M, Biever A, Jovanovic M, Schuman EM. Alternative 3'
926 UTRs modify the localization, regulatory potential, stability, and plasticity of mRNAs in
927 neuronal compartments. Neuron. 2018;98(3):495–511.

928 38. Glock C, Biever A, Tushev G, Nassim-Assir B, Kao A, Bartnik I, et al. The translatome of
929 neuronal cell bodies, dendrites, and axons. Proc Natl Acad Sci. 2021;118(43).

930 39. Dewey EB, Parra AS, Johnston CA. Loss of the spectraplakin gene Short stop induces a
931 DNA damage response in Drosophila epithelia. Sci Rep. 2020;10(1):1–13.

932 40. Sanchez-Soriano N, Travis M, Dajas-Bailador F, Gonçalves-Pimentel C, Whitmarsh AJ,
933 Prokop A. Mouse ACF7 and drosophila short stop modulate filopodia formation and
934 microtubule organisation during neuronal growth. J Cell Sci. 2009;122(14):2534–42.

935 41. Prokop A, Beaven R, Qu Y, Sánchez-Soriano N. Using fly genetics to dissect the
936 cytoskeletal machinery of neurons during axonal growth and maintenance. J Cell Sci.
937 2013;126(11):2331–41.

938 42. Valakh V, Walker LJ, Skeath JB, DiAntonio A. Loss of the spectraplakin short stop
939 activates the DLK injury response pathway in Drosophila. J Neurosci.
940 2013;33(45):17863–73.

941 43. Bennett V, Baines AJ. Spectrin and ankyrin-based pathways: metazoan inventions for
942 integrating cells into tissues. Physiol Rev. 2001;81(3):1353–92.

943 44. Thomas GH, Williams JA. Dynamic rearrangement of the spectrin membrane skeleton
944 during the generation of epithelial polarity in Drosophila. J Cell Sci.
945 1999;112(17):2843–52.

946 45. Banks GT, Fisher E. Cytoplasmic dynein could be key to understanding

947 neurodegeneration. Genome Biol. 2008;9(3):1–4.

948 46. Bianco A, Dienstbier M, Salter HK, Gatto G, Bullock SL. Bicaudal-D regulates fragile X
949 mental retardation protein levels, motility, and function during neuronal
950 morphogenesis. Curr Biol. 2010;20(16):1487–92.

951 47. Formicola N, Vijayakumar J, Besse F. Neuronal ribonucleoprotein granules: Dynamic
952 sensors of localized signals. Traffic. 2019;20(9):639–49.

953 48. Greenblatt EJ, Spradling AC. Fragile X mental retardation 1 gene enhances the
954 translation of large autism-related proteins. Science (80-). 2018;361(6403):709–12.

955 49. Lee SK, Xue Y, Shen W, Zhang Y, Joo Y, Ahmad M, et al. Topoisomerase 3β interacts
956 with RNAi machinery to promote heterochromatin formation and transcriptional
957 silencing in Drosophila. Nat Commun. 2018;9(1):4946. DOI: 10.1038/s41467-018-
958 07101-4

959 50. Wu J, Hou JH, Hsieh TS. A new Drosophila gene wh (wuho) with WD40 repeats is
960 essential for spermatogenesis and has maximal expression in hub cells. Dev. Biol.
961 2006;296:219–230. doi: 10.1016/j.ydbio.2006.04.459.

962 51. Gratz SJ, Rubinstein CD, Harrison MM, Wildonger J, O'Connor-Giles KM. CRISPR-Cas9
963 genome editing in Drosophila. Curr Protoc Mol Biol. 2015;111(1):31–2.

964 52. Port F, Bullock SL. Augmenting CRISPR applications in Drosophila with tRNA-flanked
965 sgRNAs. Nat Methods. 2016;13(10):852–4.

966 53. Cunningham F, Allen JE, Allen J, Alvarez-Jarreta J, Amode MR, Armean IM, et al.
967 Ensembl 2022. Nucleic Acids Res. 2022;50(D1):D988–95.

968 54. DeLuca SZ, Spradling AC. Efficient expression of genes in the Drosophila germline
969 using a UAS promoter free of interference by Hsp70 piRNAs. Genetics.
970 2018;209(2):381–7.

971 55. Vazquez-Pianzola P, Adam J, Haldemann D, Hain D, Urlaub H, Suter B. Clathrin heavy
972 chain plays multiple roles in polarizing the Drosophila oocyte downstream of Bic-D.
973 Development. 2014;141(9):1915–26.

974 56. Cox J, Mann M. MaxQuant enables high peptide identification rates, individualized
975 ppb-range mass accuracies and proteome-wide protein quantification. Nat

976 Biotechnol. 2008;26(12):1367–72.

977 57. Consortium U. UniProt: a worldwide hub of protein knowledge. Nucleic Acids Res.
978 2019;47(D1):D506–15.

979 58. Huber W, Von Heydebreck A, Sültmann H, Poustka A, Vingron M. Variance
980 stabilization applied to microarray data calibration and to the quantification of
981 differential expression. Bioinformatics. 2002;18(suppl_1):S96–104.

982 59. Silva JC, Gorenstein M V, Li GZ, Vissers JP. C; Geromanos, SJ Absolute quantification of
983 proteins by LCMSE: A virtue of parallel MS acquisition. Mol Cell Proteomics.
984 2006;5:144–56.

985 60. Silver JD, Ritchie ME, Smyth GK. Microarray background correction: maximum
986 likelihood estimation for the normal–exponential convolution. Biostatistics.
987 2009;10(2):352–63.

988 61. Kammers K, Cole RN, Tiengwe C, Ruczinski I. Detecting significant changes in protein
989 abundance. EuPA open proteomics. 2015;7:11–9.

990 62. Uldry A-C, Maciel-Dominguez A, Jornod M, Buchs N, Braga-Lagache S, Brodard J, et al.
991 Effect of Sample Transportation on the Proteome of Human Circulating Blood
992 Extracellular Vesicles. Int J Mol Sci. 2022;23(9):4515.

993 63. Andrews S. FastQC: a quality control tool for high throughput sequence data.
994 Babraham Bioinformatics, Babraham Institute, Cambridge, United Kingdom; 2010.

995 64. Wang L, Wang S, Li W. RSeQC: quality control of RNA-seq experiments.
996 Bioinformatics. 2012;28(16):2184–5.

997 65. Smith T, Heger A, Sudbery I. UMI-tools: modeling sequencing errors in Unique
998 Molecular Identifiers to improve quantification accuracy. Genome Res.
999 2017;27(3):491–9.

1000 66. Martin M. Cutadapt removes adapter sequences from high-throughput sequencing
1001 reads. EMBnet J. 2011;17(1):10–2.

1002 67. Kim D, Langmead B, Salzberg SL. HISAT: a fast spliced aligner with low memory
1003 requirements. Nat Methods. 2015;12(4):357–60.

1004 68. Liao Y, Smyth GK, Shi W. featureCounts: an efficient general purpose program for
1005 assigning sequence reads to genomic features. Bioinformatics. 2014;30(7):923–30.

1006 69. Love MI, Huber W, Anders S. Moderated estimation of fold change and dispersion for
1007 RNA-seq data with DESeq2. Genome Biol. 2014;15(12):1–21.

1008 70. Core R. TEAM, 2017. R: A language and environment for statistical computing. R
1009 Foundation for Statistical Computing, Vienna, Austria. Online https//www r-project
1010 org. 2022;

1011 71. Castells-Nobau A, Nijhof B, Eidhof I, Wolf L, Scheffer-de Gooyert JM, Monedero I, et
1012 al. Two algorithms for high-throughput and multi-parametric quantification of
1013 Drosophila neuromuscular junction morphology. J Vis Exp Jove. 2017;(123).

1014 72. Szklarczyk D, Franceschini A, Wyder S, Forslund K, Heller D, Huerta-Cepas J, et al.
1015 STRING v10: protein–protein interaction networks, integrated over the tree of life.
1016 Nucleic Acids Res. 2015;43(D1):D447–52.

1017 73. Stoll G, Pietiläinen OPH, Linder B, Suvisaari J, Brosi C, Hennah W, Leppä V, Torniainen
1018 M, Ripatti S, Ala-Mello S, Plöttner O, Rehnström K, Tuulio-Henriksson A, Varilo T,
1019 Tallila J, Kristiansson K, Isohanni M, Kaprio J, Eriksson JG, Raitakari OT, Lehtimäki T,
1020 Jarvelin MR, Salomaa V, Hurles M, Stefansson H, Peltonen L, Sullivan PF, Paunio T,
1021 Lönnqvist J, Daly MJ, Fischer U, Freimer NB, Palotie A. Deletion of TOP3β, a
1022 component of FMRP-containing mRNPs, contributes to neurodevelopmental
1023 disorders. Nat Neurosci. 2013 Sep;16(9):1228-1237. doi: 10.1038/nn.3484. Epub 2013
1024 Aug 4. PMID: 23912948; PMCID: PMC3986889.

1025 74. Su, S, Xue, Y., Sharov, A., Zhang, Y., Lee, S.K., Martindale, J.L., Li, W., Ku, W.L., Zhao, K.,
1026 De, S., Shen, W., Sen, P., Gorospe, M., Xu, D., Wang, W. A dual-activity topoisomerase
1027 complex regulates mRNA translation and turnover. Nucleic Acids Res 2022;
1028 50(12):7013-7033.

1029 75. Schiavo G, Greensmith L, Hafezparast M, Fisher EM. Cytoplasmic dynein heavy chain:
1030 the servant of many masters. Trends Neurosci. 2013 Nov;36(11):641-51. doi:
1031 10.1016/j.tins.2013.08.001.

1032 76. Wilkie GS, Davis I. Drosophila wingless and pair-rule transcripts localize apically by
1033 dynein-mediated transport of RNA particles. Cell. 2001 Apr 20;105(2):209-19.
1034 doi: 10.1016/s0092-8674(01)00312-9. PMID: 11336671.

1035 77. Bullock SL, Ish-Horowicz D. Conserved signals and machinery for RNA transport in
1036 Drosophila oogenesis and embryogenesis. Nature. 2001 Dec 6; 414(6864):611-6. doi:
1037 10.1038/414611a. PMID: 11740552.

1038 78. Foe, VE, and Alberts, BM. Studies of nuclear and cytoplasmic behavior in the five
1039 mitotic cycles that precede gastrulation in *Drosophila* embryogenesis. J. Cell Sci. 1983;
1040 **61,** 31-70.

1041 79. Lee, MT, Bonneau, AR, and Giraldez, AJ. Zygotic genome activation during the
1042 maternal-to-zygotic transition. Annu. Rev. Cell Dev. Biol. 2014; 30, 581-613

1043 80. Tadros, W and Lipshitz, HD. The maternal-to-zygotic transition: a play in two acts.
1044 Development 2009; 136, 3033-3042.

1045 81. Vazquez-Pianzola, P, Schaller, B, Colombo, M, Beuchle, D, Neuenschwander, S, Marcil,
1046 A, Bruggmann, R, and Suter, B. The mRNA transportome of the BicD / Egl transport
1047 machinery. RNA Biology 2017; 14:1, 73-89, DOI: 10.1080/15476286.2016.1251542

1048 82. Vazquez-Pianzola, P, Beuchle, D, Saro, G, Hernández, G, Maldonado, G, Brunßen, D,
1049 Meister, P, and Suter, B. Female meiosis II and pronuclear fusion require the
1050 microtubule transport factor Bicaudal D. Development. 2022 Jul 1;
1051 149(13):dev199944. doi: 10.1242/dev.199944.

1052 83. Thomas, CM, and Kiehart, DP. β_{Heavy}-spectrin has a restricted tissue and subcellular
1053 distribution during Drosophila embryogenesis. Development 1994; 120:7, 2039-2050.
1054 Doi: 10.1242/dev.120.7.2039

1055 84. Rahman FU, Kim YR, Kim EK, Kim HR, Cho SM, Lee CS, Kim SJ, Araki K, Yamamura KI,
1056 Lee MN, Park SG, Yoon WK, Lee K, Won YS, Kim HC, Lee Y, Lee HY, Nam KH.
1057 Topoisomerase IIIβ Deficiency Induces Neuro-Behavioral Changes and Brain
1058 Connectivity Alterations in Mice. Int J Mol Sci. 2021 Nov 26;22(23):12806. doi:
1059 10.3390/ijms222312806.

1060 85. Zhu X, Joo Y, Bossi S, McDevitt RA, Xie A, Wang Y, Xue Y, Su S, Lee SK, Sah N, Zhang S,
1061 Ye R, Pinto A, Zhang Y, Araki K, Araki M, Morales M, Mattson MP, van Praag H, Wang
1062 W. Tdrd3-null mice show post-transcriptional and behavioral impairments associated
1063 with neurogenesis and synaptic plasticity. Prog Neurobiol. 2024 Feb;233:102568. doi:
1064 10.1016/j.pneurobio.2024.102568.

1065 86. Joo Y, Xue Y, Wang Y, McDevitt RA, Sah N, Bossi S, Su S, Lee SK, Peng W, Xie A, Zhang
1066 Y, Ding Y, Ku WL, Ghosh S, Fishbein K, Shen W, Spencer R, Becker K, Zhao K, Mattson
1067 MP, van Praag H, Sharov A, Wang W. Topoisomerase 3β knockout mice show
1068 transcriptional and behavioural impairments associated with neurogenesis and
1069 synaptic plasticity. Nat Commun. 2020 Jun 19;11(1):3143. doi: 10.1038/s41467-020-
1070 16884-4.

1071 87. Su S, Xue Y, Lee SK, Zhang Y, Fan J, De S, Sharov A, and Wang W. A dual-activity
1072 topoisomerase complex promotes both transcriptional activation and repression in
1073 response to starvation. Nucleic Acids Research 2023, Vol. 51, No. 5 2415–2433.
1074 doi.org/10.1093/nar/gkad086

1075 88. Saha S, Sun Y, Huang SN, Baechler SA, Pongor LS, Agama K, Jo U, Zhang H, Tse-Dinh YC,
1076 Pommier Y. DNA and RNA Cleavage Complexes and Repair Pathway for TOP3B RNA-
1077 and DNA-Protein Crosslinks. Cell Rep. 2020 Dec 29;33(13):108569. doi:
1078 10.1016/j.celrep.2020.108569.

1079 89. Huang L, Wang Z, Narayanan N, Yang Y. Arginine methylation of the C-terminus RGG
1080 motif promotes TOP3B topoisomerase activity and stress granule localization. Nucleic
1081 Acids Res. 2018 Apr 6;46(6):3061-3074. doi: 10.1093/nar/gky103.

1082 90. Yang X, Saha S, Yang W, Neuman KC, Pommier Y. Structural and biochemical basis for
1083 DNA and RNA catalysis by human Topoisomerase 3β. Nat Commun. 2022 Aug 9;
1084 13(1):4656. doi: 10.1038/s41467-022-32221-3.

1085 91. Patro, R., Duggal, G., Love, M. *et al.* Salmon provides fast and bias-aware
1086 quantification of transcript expression. *Nat Methods* **14**, 417–419 (2017).
1087 https://doi.org/10.1038/nmeth.4197

1088 92. Zhang, G., Xu, Y., Wang, X. *et al.* Dynamic FMR1 granule phase switch instructed by
1089 m6A modification contributes to maternal RNA decay. *Nat Commun* **13**, 859 (2022).
1090 https://doi.org/10.1038/s41467-022-28547-7

1091 93. Kwan, KY, and Wang, JC. Mice lacking DNA topoisomerase IIIbeta develop to maturity
1092 but show a reduced mean lifespan. Proc Natl Acad Sci USA 98(10):5717-21 (2001).
1093 DOI: 10.1073/pnas.101132498

1094 94. Suter, B. RNA localization and transport. BBA - Gene Regulatory Mechanisms 1861;
1095 10, 938-951 (2018). doi.org/10.1016/j.bbagrm.2018.08.004

1096

1097 **Figure legends**

1098 **Fig. 1. Effect of the *Top3β* mutations on the transcriptome of 0-2 hrs. old embryos. A)**
1099 The left and central panels show the changes compared to the wild-type (WT) transcriptome
1100 using adjusted p-values (Adjp) <0.05 and log2-fold change <-1 (downregulated) and >1
1101 (upregulated). The Venn diagram shows also the allocation of the data to the 3 different
1102 mutants. Using the more stringent criteria Adjp <0.0002 and log2-fold change <-1, the right
1103 Venn diagram shows the fractions of the genes with reduced transcript levels and which
1104 mutant showed the reduction. n: is the number of different genes identified in the three
1105 mutants. **B)** Differentially expressed transcript isoforms in the $Top3\beta^{26}$ null mutant compared
1106 to the wild type (WT). Adjp <0.05 and absolute log2-fold change ≥1. The Venn diagram shows
1107 which fraction is also differentially expressed in the point mutants when analyzed with the
1108 same stringency parameters (left panel). The fractions of the differentially expressed transcript
1109 isoforms expressed at lower levels in the mutants are shown in the right diagram. **C)-E)** RNA
1110 features of the genes, which produce the transcript isoforms, that depend on *Top3β* to reach
1111 normal expression levels. **C)** Transcript isoforms from genes that produce long UTRs are over-
1112 represented in the group of RNAs that depend on *Top3β* and its Tyr^{332} (Y332) residue to reach
1113 normal expression levels. **D)** Transcript isoforms from genes that encode longer CDS are
1114 expressed at higher levels in the wild type than in the $Top3\beta^{26}$ and $Top3\beta^{Y332F}$ mutants. **E)**
1115 Transcript isoforms from genes that produce longer pre-mRNAs are expressed at higher levels
1116 in the wild type than in the $Top3\beta^{26}$ and $Top3\beta^{Y332F}$. Expression levels were compared to the
1117 $Top3\beta^{+}$ (WT) control in 0-2 hrs. old embryos. p-value <0.0001=****, p-value <0.001=***, p-
1118 value <0.01=**, p-value <0.05=*. n=50 for the null mutant $Top3\beta^{26}$ and $Top3\beta^{Y332F}$ and n=5 for
1119 $Top3\beta^{\Delta RGG}$.

1120

1121 **Fig. 2. Overlap between downregulated embryonic RNAs in $Top3\beta^{26}$ and the fly**
1122 **homologs of differentially expressed RNAs in several cancers and neurological**
1123 **diseases associated with human *Top3β*. A, B)** Venn diagram of the genes shared between

1124 the list of down-regulated RNAs in *Top3β*^{26} embryos and the fly homologs of differentially
1125 expressed RNAs of the listed diseases. Numbers and frequencies are listed. The probability
1126 of random overlap is shown in % at the bottom left of each Venn diagram. **C)** Drosophila genes
1127 depending on *Top3β* for normal expression levels in embryos were placed into a Venn diagram
1128 such that their position shows in which neurological disease their homologs differentially
1129 expressed (note that JME was not included). *Rop* appeared in all lists. **D)** Drosophila genes
1130 depending on *Top3β* for normal expression levels in embryos were placed into a Venn diagram
1131 such that their position shows in which cancer their homologs are differentially expressed. **E)**
1132 List of the 50 genes that depend on *Drosophila Top3β* for their normal expression levels in
1133 embryos and whose homologs are also affected in all listed cancers associated with human
1134 *Top3β* alterations.

1135

1136 **Fig 3: Characteristics of embryonic RNA targets of Top3β::eGFP**. **A)** Longer RNAs are
1137 more likely targets of the enzymatic activity of Top3β because they are more enriched in the
1138 IP with the wild-type *Top3β* compared to the *Top3β*^{Y332F}. r measures the strength of the
1139 correlation and p stands for p-value. **B-E)** Transcript features of the top 46 embryonic RNA
1140 targets of Top3β::eGFP. The complete sets of RNAs detected in the wild-type RNA-IP served
1141 as the standard. p-value <0.0001=****, p-value <0.001=***, p-value <0.01=**, p-value <0.05=*.

1142

1143 **Fig. 4: Comparing Drosophila Top3β targets and effects to the corresponding**
1144 **FMR1/FMRP and mammalian Top3β data. A)** A previous mammalian study produced a list
1145 of overlapping mouse FMRP targets in brain extracts and Top3β targets in HeLa cells (1). The
1146 Venn diagram compares the list of Drosophila homologs of these mammalian targets to our
1147 list of direct targets of Top3β. The list of the Drosophila homologs that were also found in both
1148 mammalian interactor screens is shown with the characteristics of the Drosophila gene. The
1149 length measurements stem from the longest pre-mRNA isoforms (**Supplementary Table**

1150 **S11**). **B)** Comparing RNASeq data from 0-2 hrs old embryos from the *Top3β*^{26} null mutant
1151 **(**Adjp < 0.0002; log2-fold change <-1 and >1, respectively, according to **Supplementary Table**
1152 **S1)** and the *FMR1* mutant (92). The analysis considers reads per gene. Lists of the genes
1153 identified in the overlapping datasets are presented in the supplements **(Supplementary**
1154 **Table S13). C)** Genes encoding transcript isoforms that depend on *Top3β* for their normal
1155 accumulation in young embryos (**Supplementary Table S4**) and transcripts that depend on
1156 *FMR1* for their translation in quiescent oocytes (48). The Venn diagram shows the overlap
1157 between the two datasets and the genes in the overlap are listed. **D)** Comparing RNASeq data
1158 from 0-2 hrs old *Top3β*^{26} embryos **(**Adjp <0.0002; log2-fold change <-1**; Supplementary**
1159 **Table S1)** and the *FMR1* RNAi effect on translational repression (48).

1160

1161 **Fig. 5. Expression and localization of gene products of Top3β targets.** The posterior pole
1162 of the embryos is shown to the right. *shot* mRNA and Shot protein localization in the posterior
1163 part of syncytial (*shot* mRNA) and cellularizing (Shot protein) wild-type embryos in the different
1164 *Top3β* mutants. Lower signal levels and less localized signals were seen in the null and
1165 *Top3β*^{Y332F}. Both were less reduced in *Top3β*$^{\Delta RGG}$ mutant embryos. Note the *shot* mRNA
1166 localization in the pole cells in the wild type and *Top3β*$^{\Delta RGG}$ mutant. Dhc64C localization at the
1167 posterior side of the somatic part of the embryo (arrowhead) was not detectable in the null
1168 mutant and *Top3β*^{Y332F} and reduced in *Top3β*$^{\Delta RGG}$ mutant embryos. Kst localization at the
1169 apical membrane (arrowhead) was reduced in null mutants and *Top3β*^{Y332F} compared to the
1170 wild type. Top3β protein is localized similarly to its targets. It is, however, absent from the null
1171 mutant which reveals the background levels of the staining. Note that Top3β is also nuclear in
1172 the wild type and *Top3β*^{Y332F} but absent from nuclei in the *Top3β*$^{\Delta RGG}$ embryo. Imaging settings
1173 were identical for the staining for the same protein and mRNA, respectively, in the different
1174 genotypes except for the insets which were overexposed to reveal the embryo. The scale bar
1175 is 10μm for the *shot* mRNA pictures and 20μm for the other micrographs.

1176

1177 **Fig. 6: Aging effects of *Top3β* mutants. A)** Climbing assays of wild type, *Top3β*$^{\Delta RGG}$,
1178 *Top3β*^{Y332F}, and *Top3β*^{26} flies. A two-way ANOVA analysis was performed. The graph bars
1179 show the mean climbing index (C.I.) for the different genotypes. Error bars represent the
1180 standard error of the mean (S.E.M). Each dot represents a calculated individual C.I. The
1181 adjusted p-values for each significant difference are indicated on the graph. (p-value
1182 <0.0001=****, p-value <0.001=***, p-value <0.01=**, p-value <0.05=*.) **B)** In adults, null
1183 mutant NMJs contain more branches than the wild type, indicative of a compensatory
1184 mechanism. Arrowheads point to the lost synaptic integrity of the dorsal longitudinal flight
1185 muscle (DLM). NMJ synapses were visualized by staining motor neurons with anti-HRP
1186 antibodies. The progressive denervation of the DLM is particularly evident in the null and the
1187 *Y332F* mutant in the adult thoracic NMJs. The scale bar represents 20μm. All panels show
1188 maximum intensity projections with a z-step size of 0.7μm. **C)** Life span shortening by *Top3β*
1189 mutations. *Top3β*^{26}null and *Top3β*^{Y332F} mutants reduce long-term survival. *Top3β*$^{\Delta RGG}$, which
1190 showed only a minor reduction compared to a wild-type strain in other experiments, served as
1191 a control because it was induced in the same background as *Top3β*^{Y332F}.

1192

1193 **Fig. 7: *Top3β* activities toward (G4C2)$_{49}$ repeat RNAs in the eye.** Expression of the UAS-
1194 (G4C2)$_{49}$ transgene in wild-type (+) and *Top3β* mutant flies using the GMR-GAL4 driver.
1195 *Top3β*$^{\Delta RGG}$ caused mild disruptions, the *Top3β*^{26} and *Top3β*^{Y332F} mutants caused strong
1196 degeneration. Shown are data from one experiment carried out in parallel; data were
1197 reproduced in a total of three or more independent experiments. All *Top3β* mutants enhanced
1198 the degenerative phenotype of the (G4C2)$_{49}$ RNA. UAS-(G4C2)$_{49}$ and GMR-GAL4 lines were
1199 heterozygous. + indicates the control genotype *Top3β*$^{+}$; the mutant alleles are indicated.

1200

Figure 1

A

downregulated in

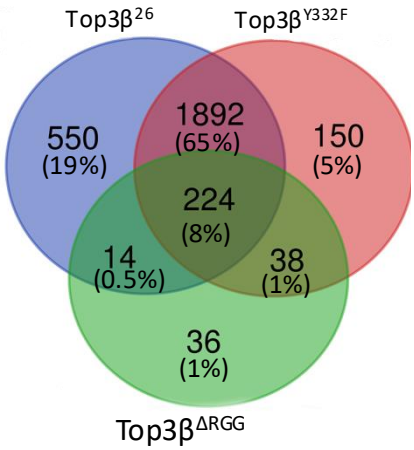

upregulated in

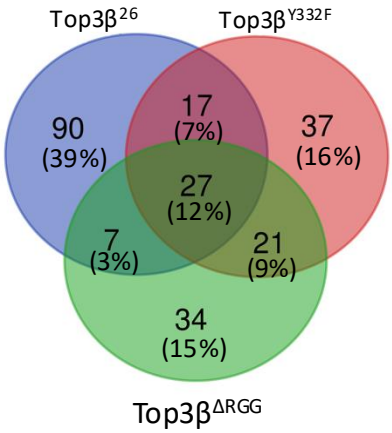

downregulated in

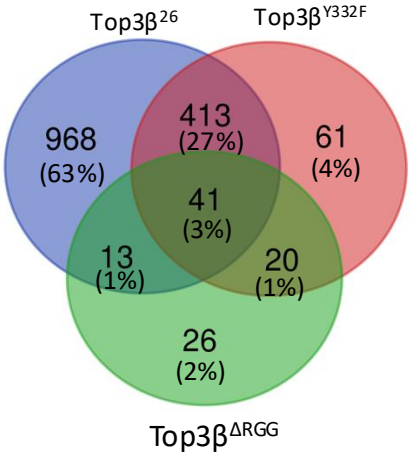

Adjp <0.05

log2-fold change <-1; n=2904 log2-fold change >1; n=233

Adjp <0.0002

log2-fold change <-1; n=1542

B

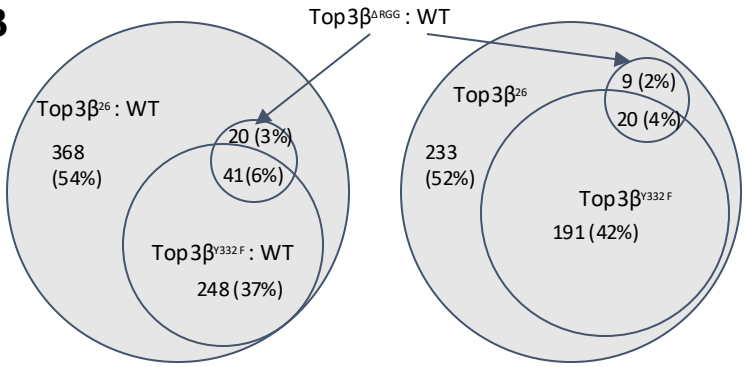

C

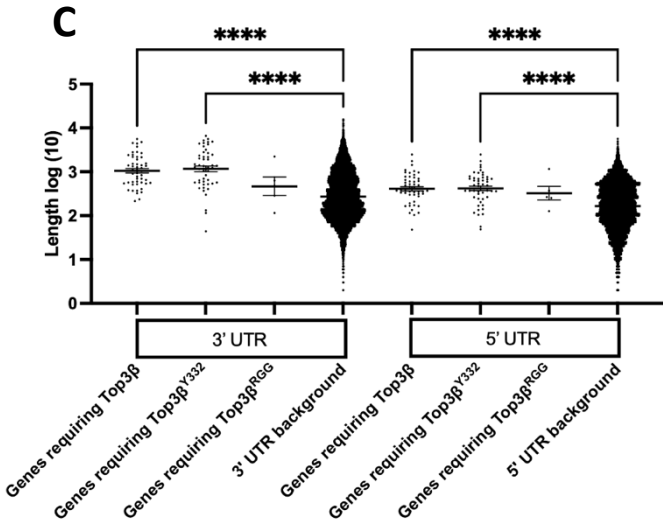

D

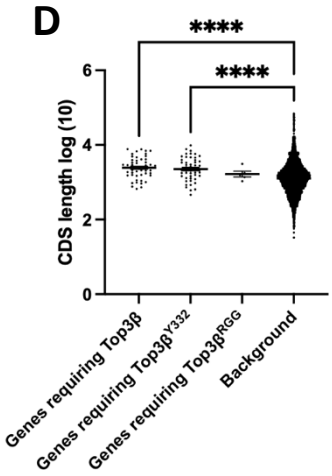

E

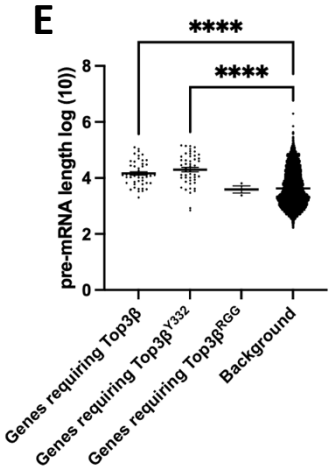

Figure 2

A **Neurological diseases**

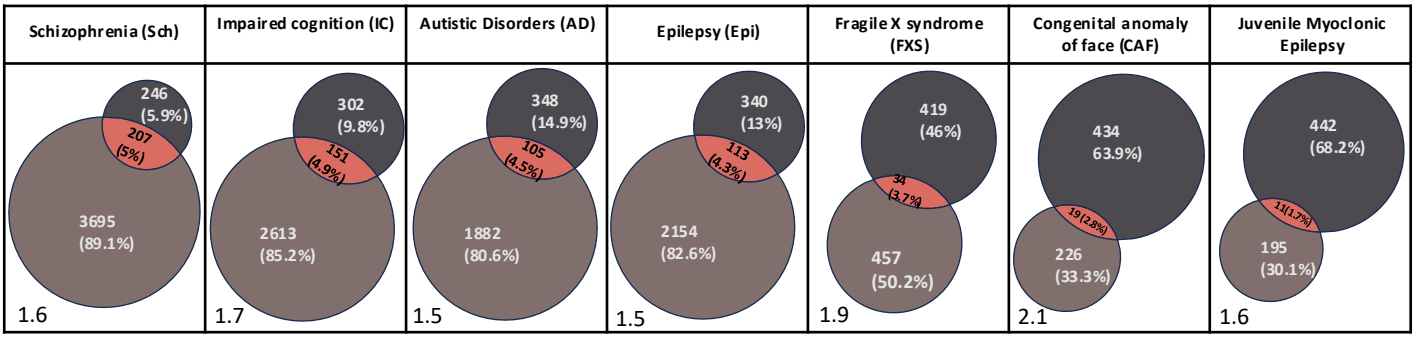

B **Cancers**

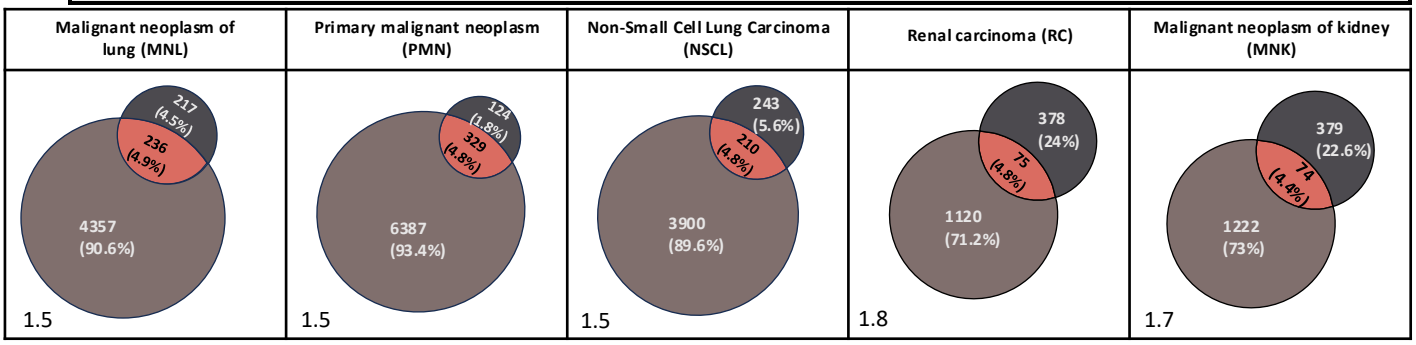

Downregulated RNAs in *Top3β*^{26} that are not shared with the orthologs of the differentially expressed disease RNAs.

Fly orthologs of disease RNAs shared between the respective disease and the downregulated RNAs in *Top3β*^{26} mutants.

Fly orthologues of differentially expressed RNAs for each disease that are not down-regulated in *Top3β*^{26} embryos.

C

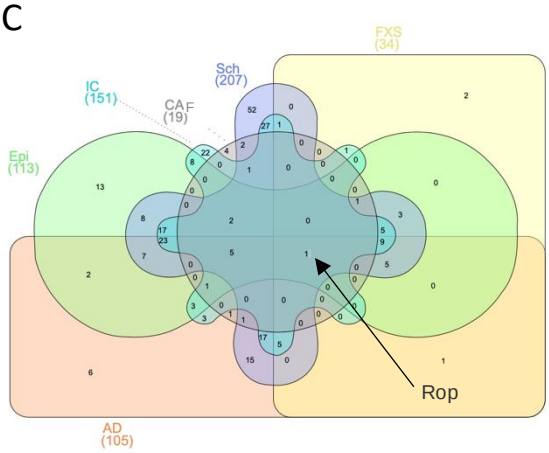

D

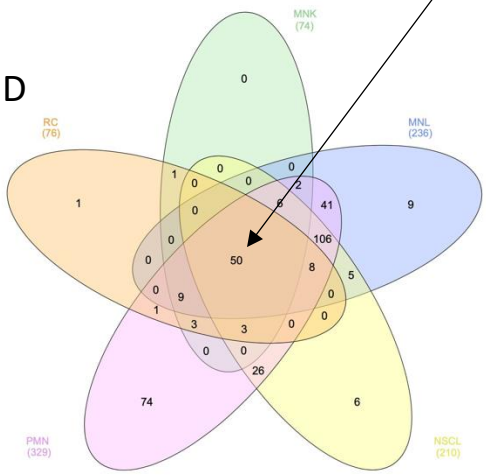

E

Glut1	Cam	myo
CG17646	Tob	ftz-f1
CG31689	dpp	CG12163
kuz	Btk29A	MTA1-like
Syt7	Rb97D	Src42A
mfas	Fak	Diap1
snu	nrv2	ham
Moe	Orct2	Pdp1
Mbs	CG11961	RhoGAP9 2B
cnc	mld	Nrt
Pak	rl	crb
Zdhhc8	CG4313	B52
aPKC	gfzf	RtGEF
Hnf4	Fas1	SERCA
rdx	RapGAP1	Met
nmo	EcR	SP1029
CG10960	Mkk4	

Figure 3

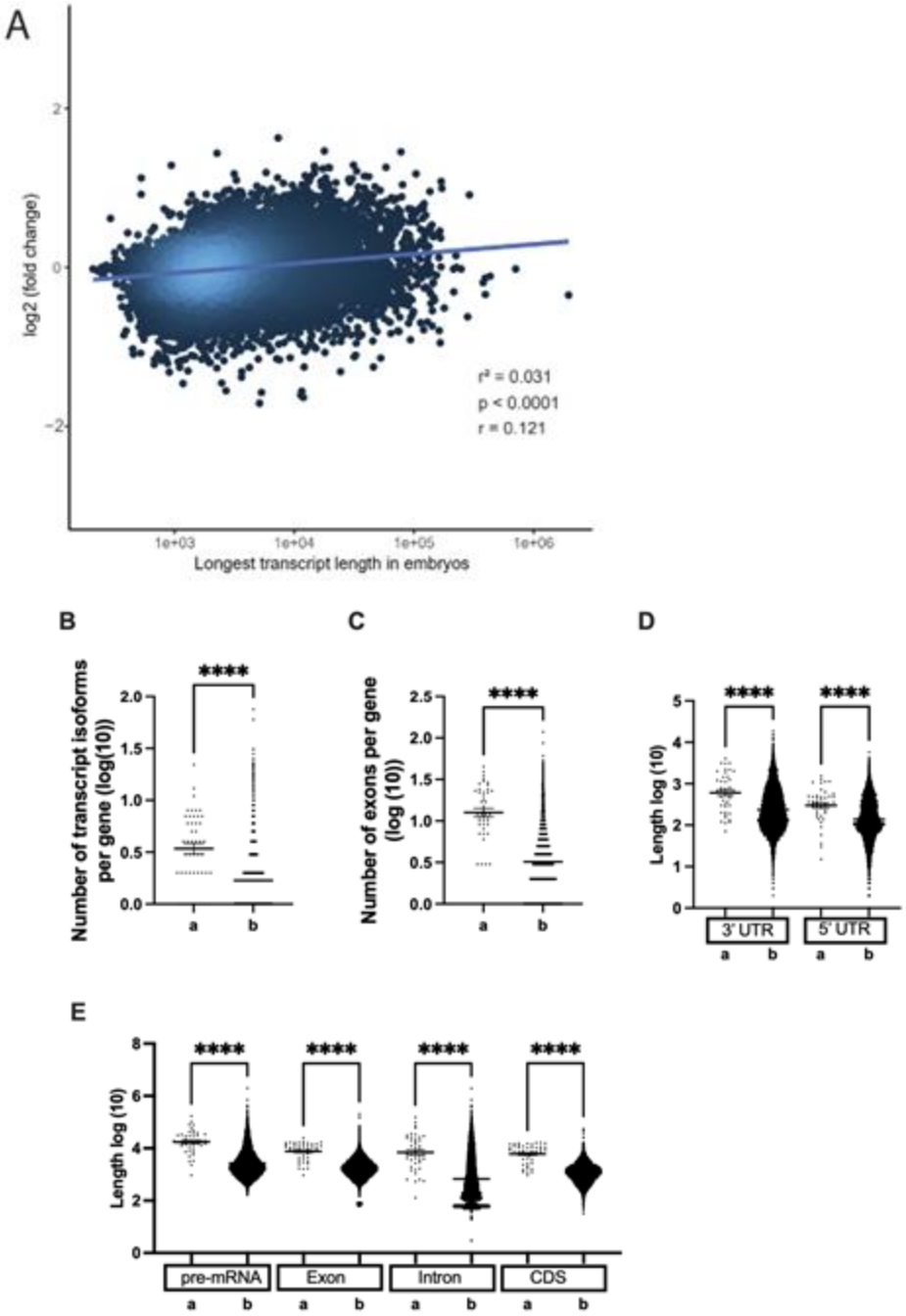

a) The top 46 RNAs enriched in Top3β::eGFP embryonic RNA-IP
b) Complete set of embryonic RNAs detected in Top3β::eGFP RNA-IP

Figure 4

A

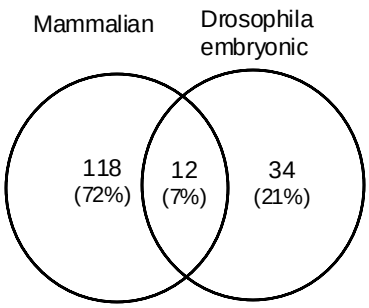

Homologous targets in "mammalian", and "Drosophila embryo"

gene	isoform	pre-mRNA	exon	intron	CDS	3UTR	5UTR
pcx	3	12750	12119	631	10251	1450	415
shot	22	77874	17845	60029	16224	1117	501
Bruce	5	19315	15702	3613	14928	605	166
FASN1	2	11580	8622	2958	7314	675	630
HERC2	1	17853	15917	1936	14736	693	485
Myo10A	4	33207	10459	22748	9162	579	715
kst	7	31274	13314	17960	12621	362	328
alpha-Spec	4	16844	8317	8527	7341	697	276
Dhc64C	8	18320	14401	3919	13983	299	116
Prosap	4	80447	8827	71620	5418	1870	1536
Smr	4	58242	24848	33568	10821	3097	1280
sev	1	14859	8171	6688	7662	280	226

B

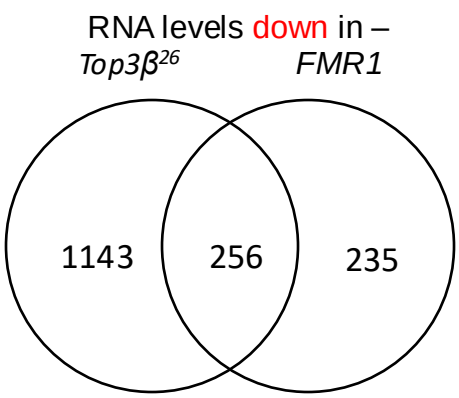

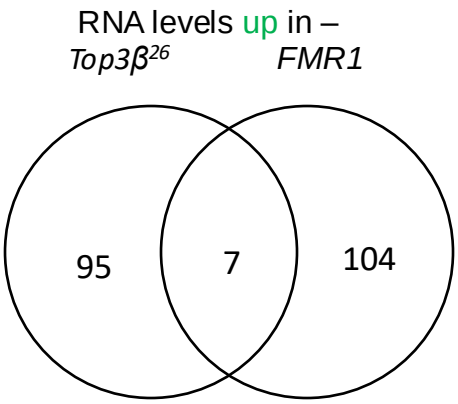

C

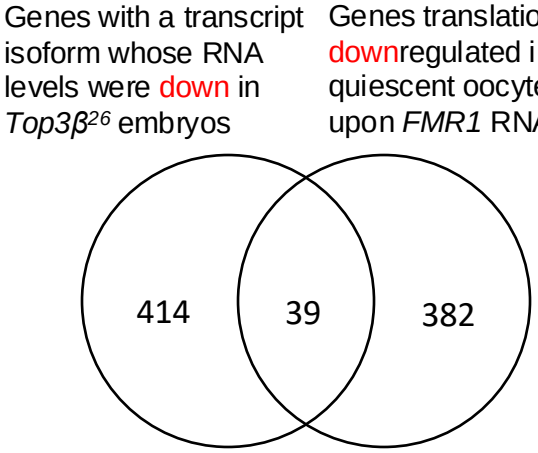

Name of genes downregulated by both procedures

PCB	spir	shi	spri
svr	Atpalpha	Mrtf	Hsc70-3
spen	CG10960	mld	CG31729
oys	toc	Exn	Ack-like
Abl	raskol	Ptp99A	BicD
Glut1	Med	Pde11	Nost
CG43783	Dys	fs(1)h	ctrip
slif	Crag	CG2747	CG13917
Mbs	mtd	stx	SP1029
cnc	CG2818	cana	

D

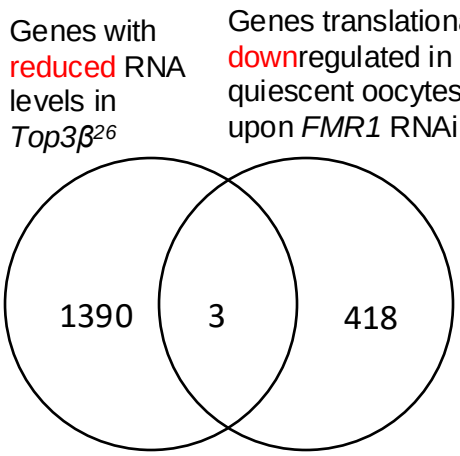

Name of genes found in both datasets

CG31673
vari
wisp

Figure 5

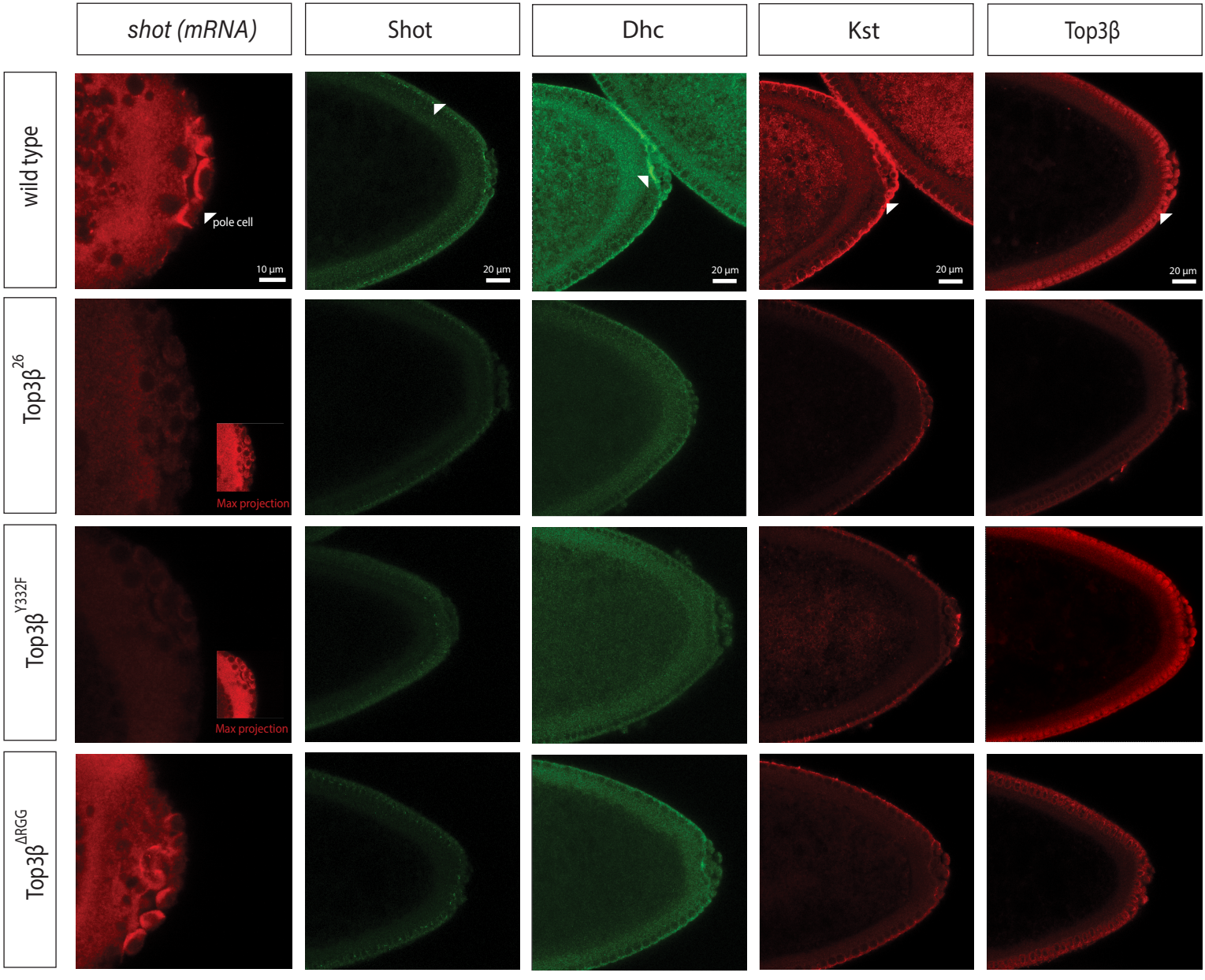
shot (mRNA)
Shot
Dhc
Kst
Top3β
wild type
Top3β26
Top3βY332F
Top3βΔRGG
pole cell
10 µm
20 µm
Max projection

Figure 6

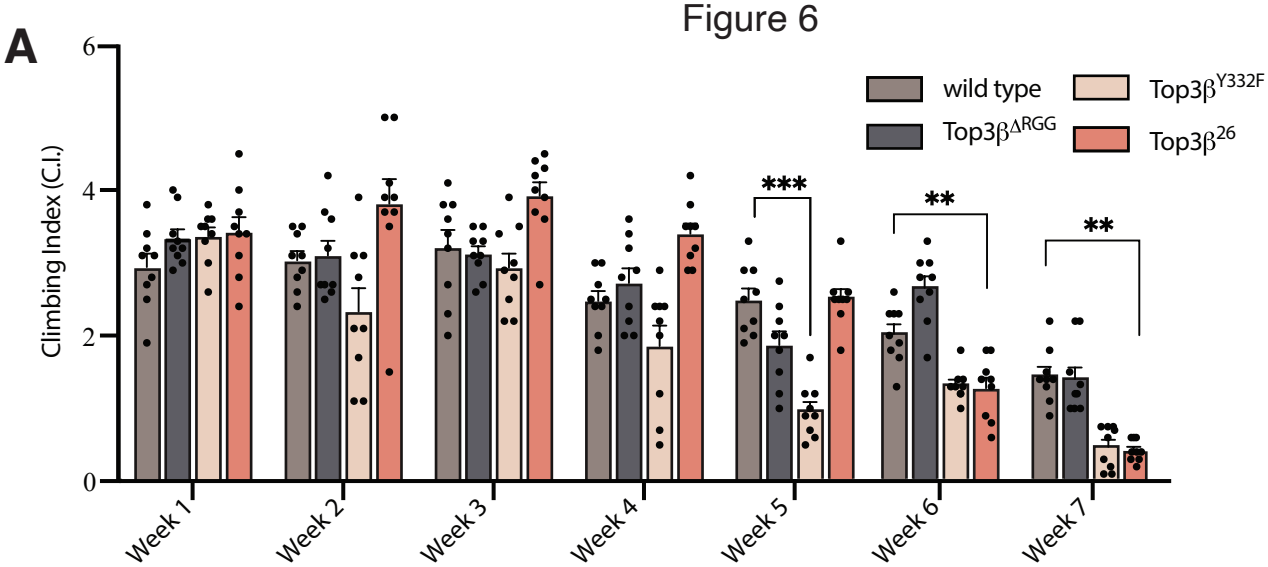
A
Climbing Index (C.I.)
6
4
2
0
wild type
Top3β^Y332F
Top3β^ΔRGG
Top3β^26
***
**
**
Week 1
Week 2
Week 3
Week 4
Week 5
Week 6
Week 7

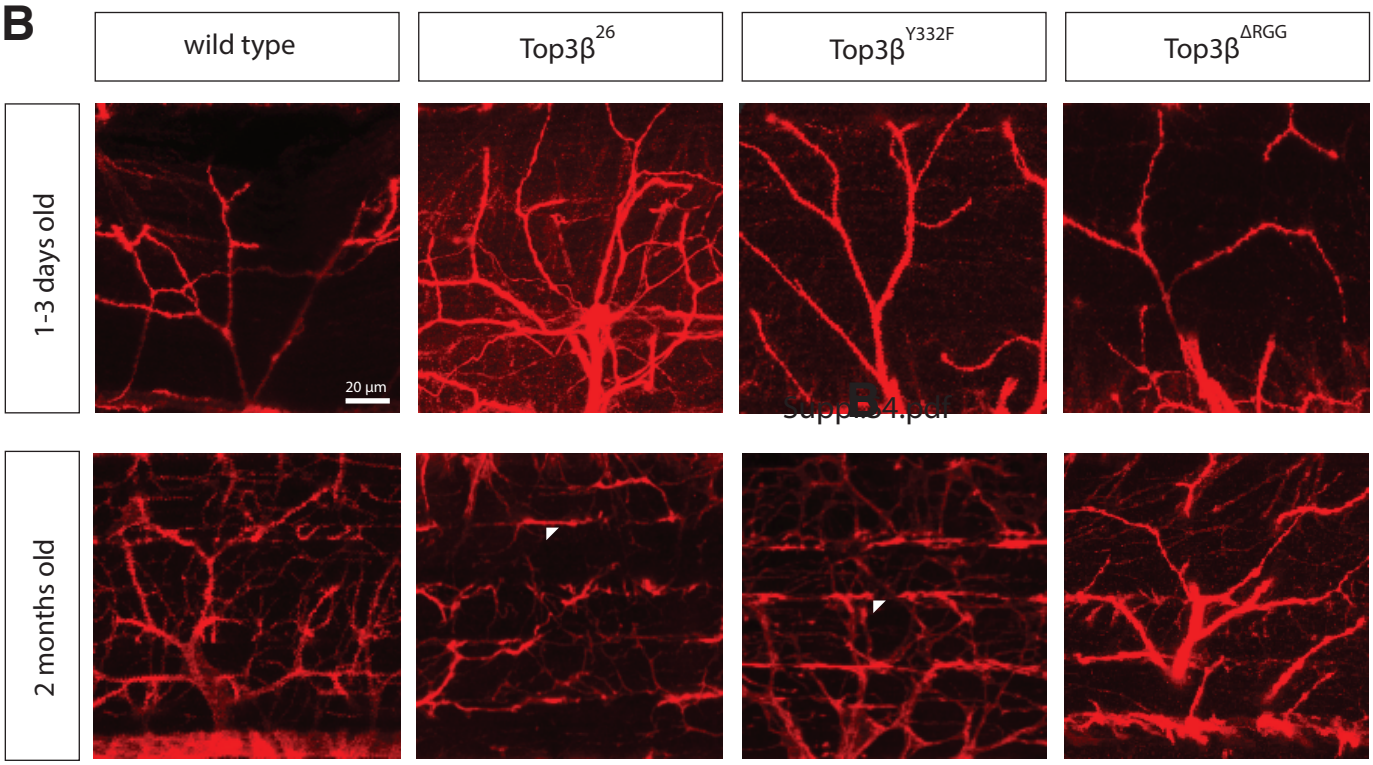
B
wild type
Top3β^26
Top3β^Y332F
Top3β^ΔRGG
1-3 days old
2 months old
20 µm

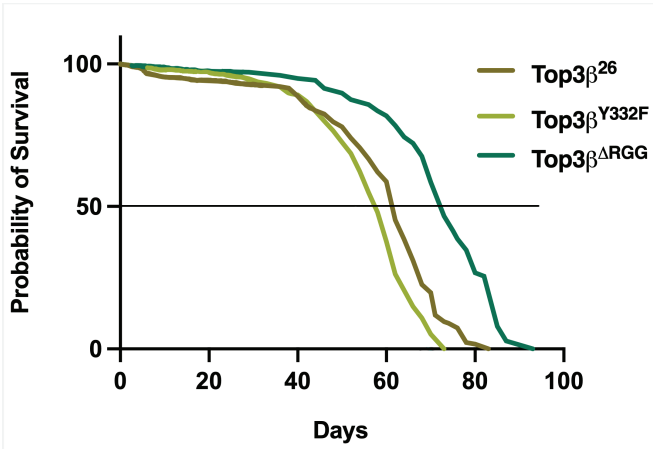
C
Probability of Survival
100
50
0
0
20
40
60
80
100
Days
Top3β^26
Top3β^Y332F
Top3β^ΔRGG

Figure 7

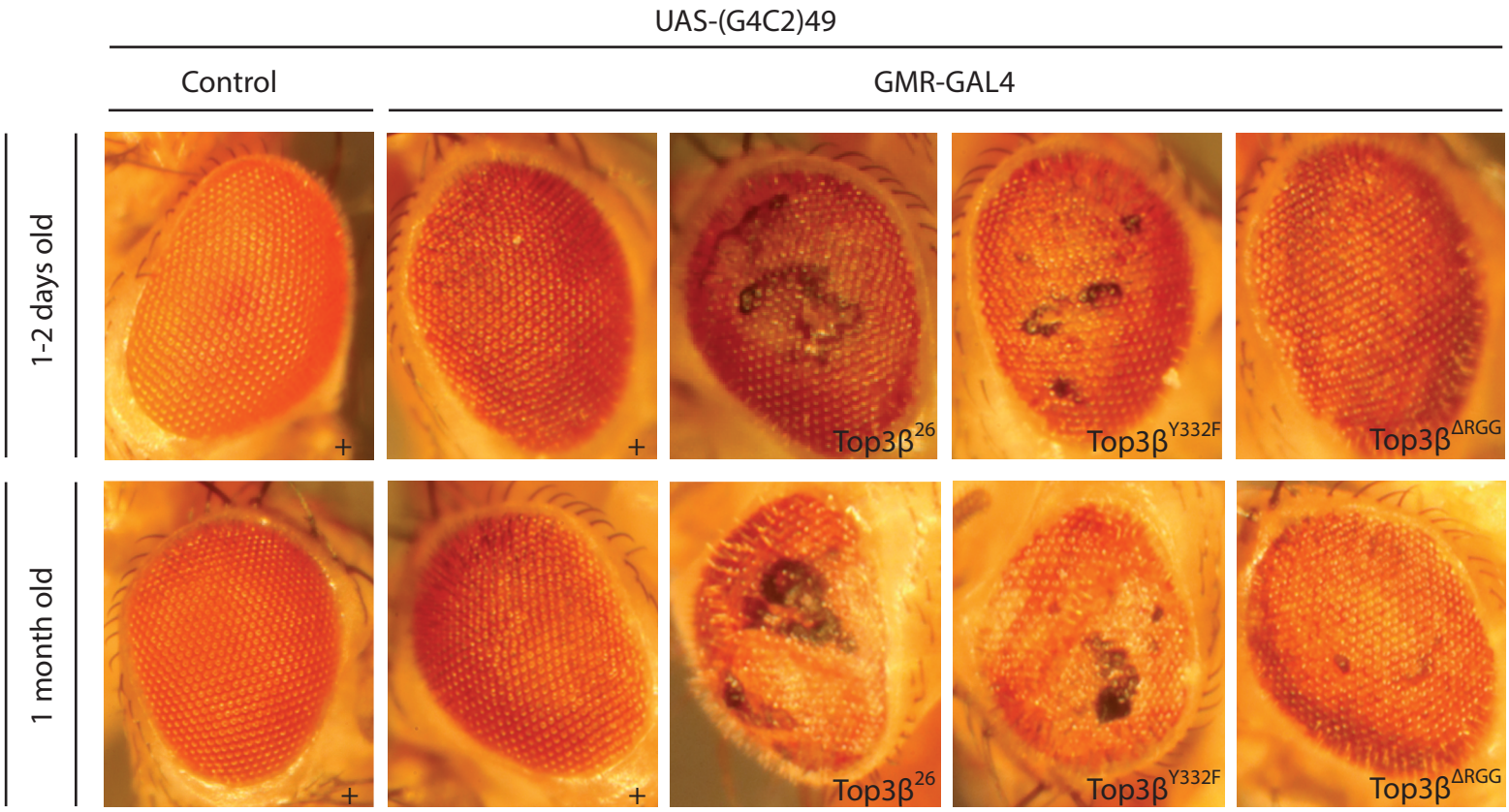
UAS-(G4C2)49
Control
GMR-GAL4
1-2 days old
1 month old
+
+
Top3β26
Top3βY332F
Top3βΔRGG
+
+
Top3β26
Top3βY332F
Top3βΔRGG

Figure S1

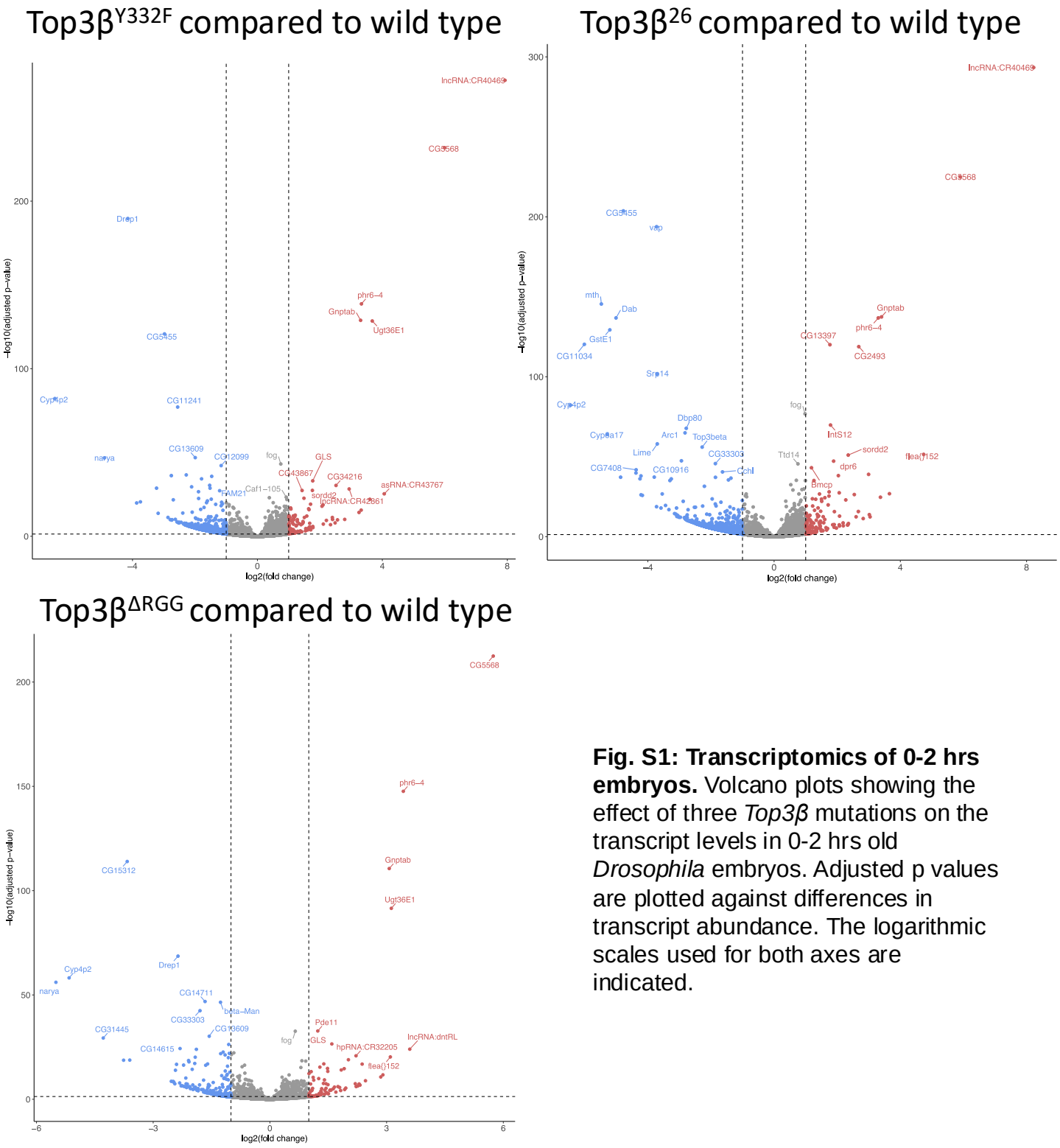

Fig. S1: Transcriptomics of 0-2 hrs embryos. Volcano plots showing the effect of three *Top3β* mutations on the transcript levels in 0-2 hrs old *Drosophila* embryos. Adjusted p values are plotted against differences in transcript abundance. The logarithmic scales used for both axes are indicated.

Figure S2

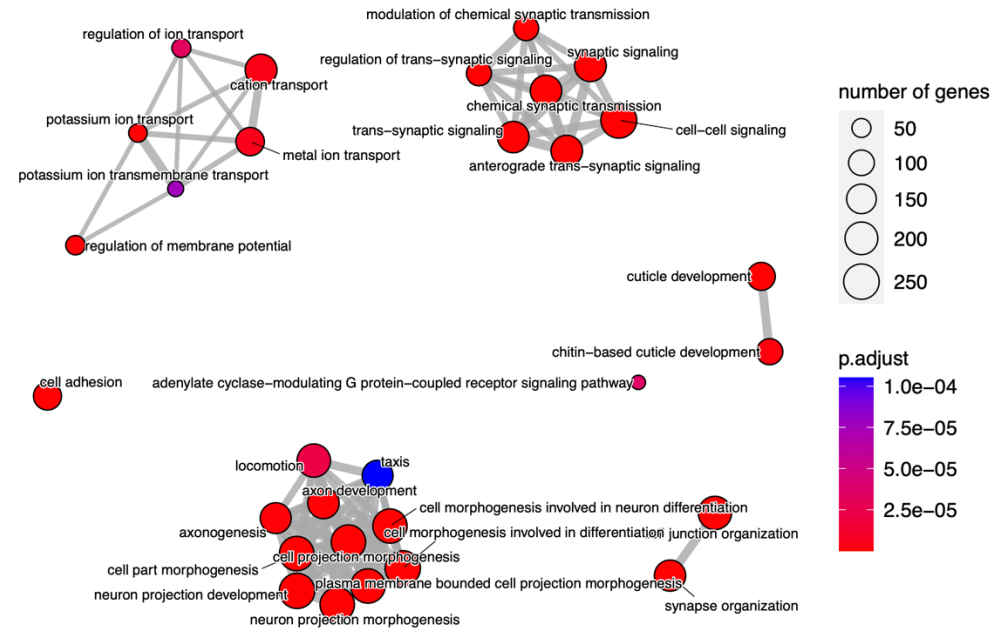

Top3β^{Y332F}
enzymatic mutation

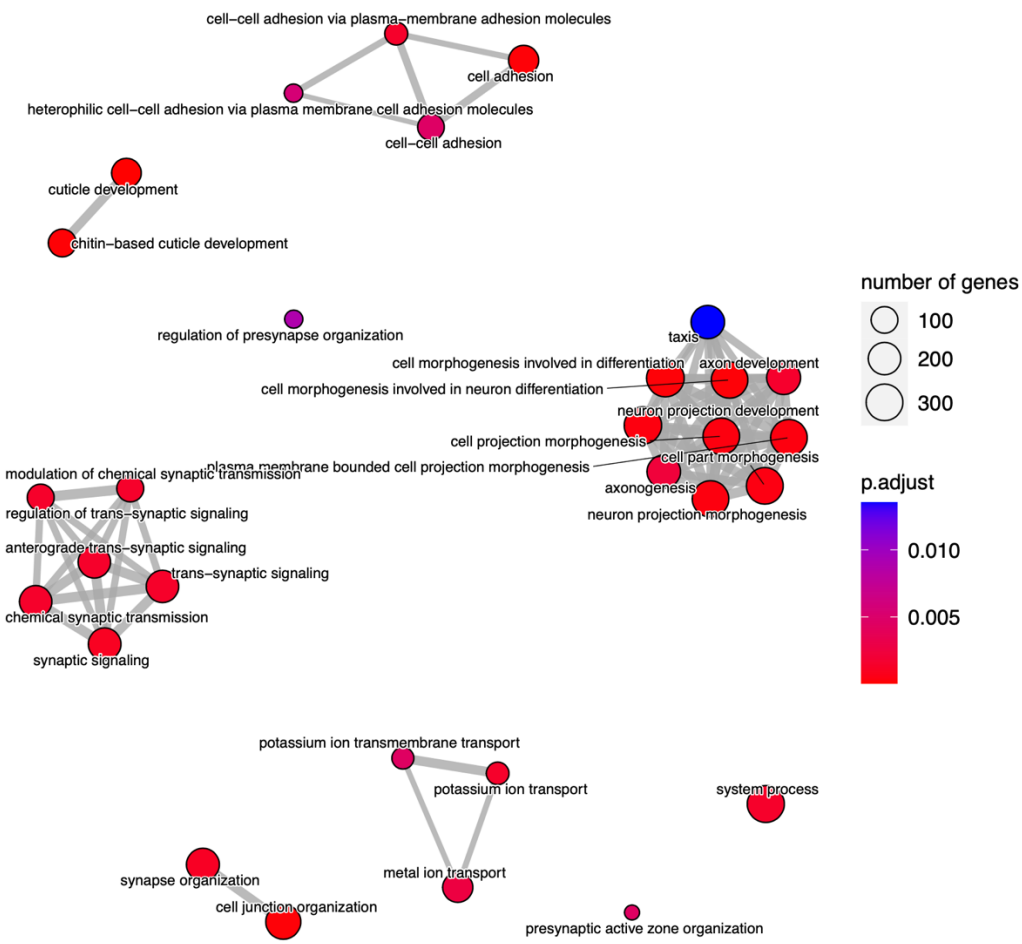

Top3β^{26}
null mutation

Fig. S2: Gene Ontology Biological Processes.
The enzymatic dead mutant *Top3β*^{Y332F} and the null mutant *Top3β*^{26} show very similar effects on biological processes, indicating that the Tyr in the active site plays a crucial role in the expression of normal levels of specific mRNAs at the early embryonic stage. The *Top3β*$^{\Delta RGG}$ mutant did not reveal enrichment terms.

Figure S3

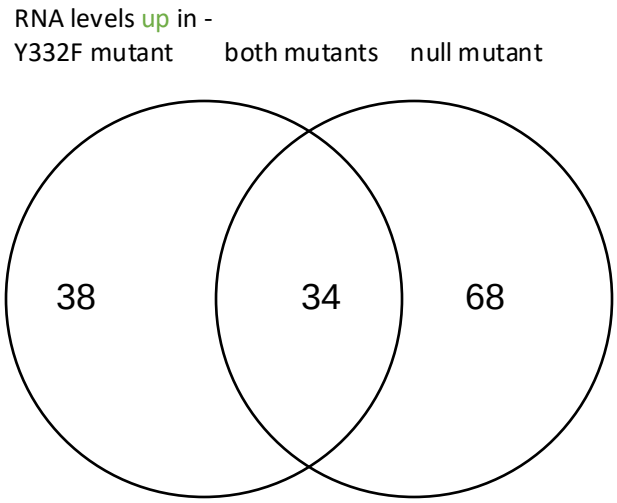

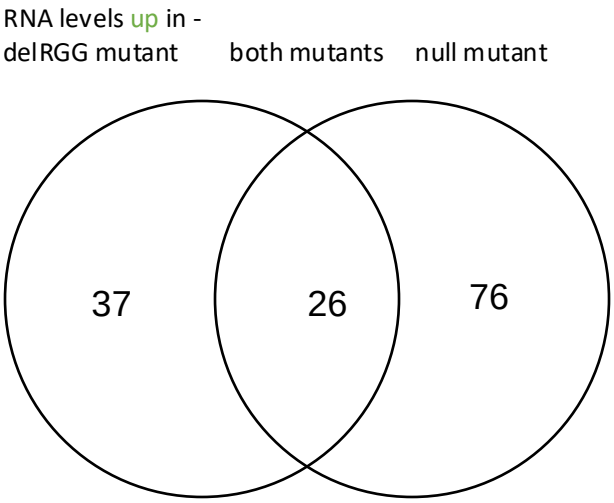

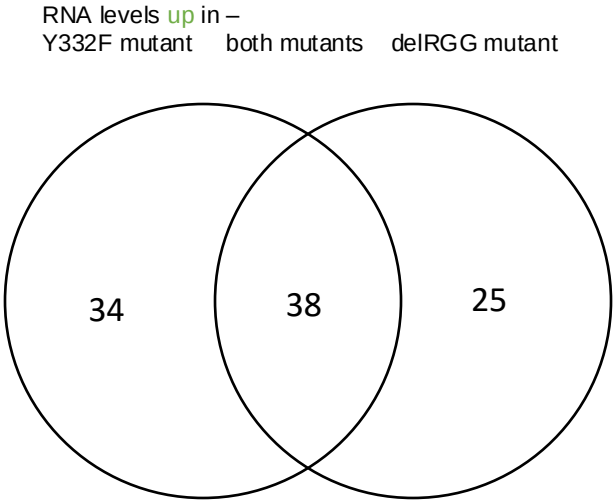

Fig. S3: RNA levels elevated in the *Top3β* mutants. Genes showing higher transcript levels in 0-2 hrs old embryos mutant for *Top3β* (compared to their wild-type expression). Adjp <0.0002; log2 fold changes ≥1. The Venn diagram shows the pairwise overlap between the different mutants.

Figure S4

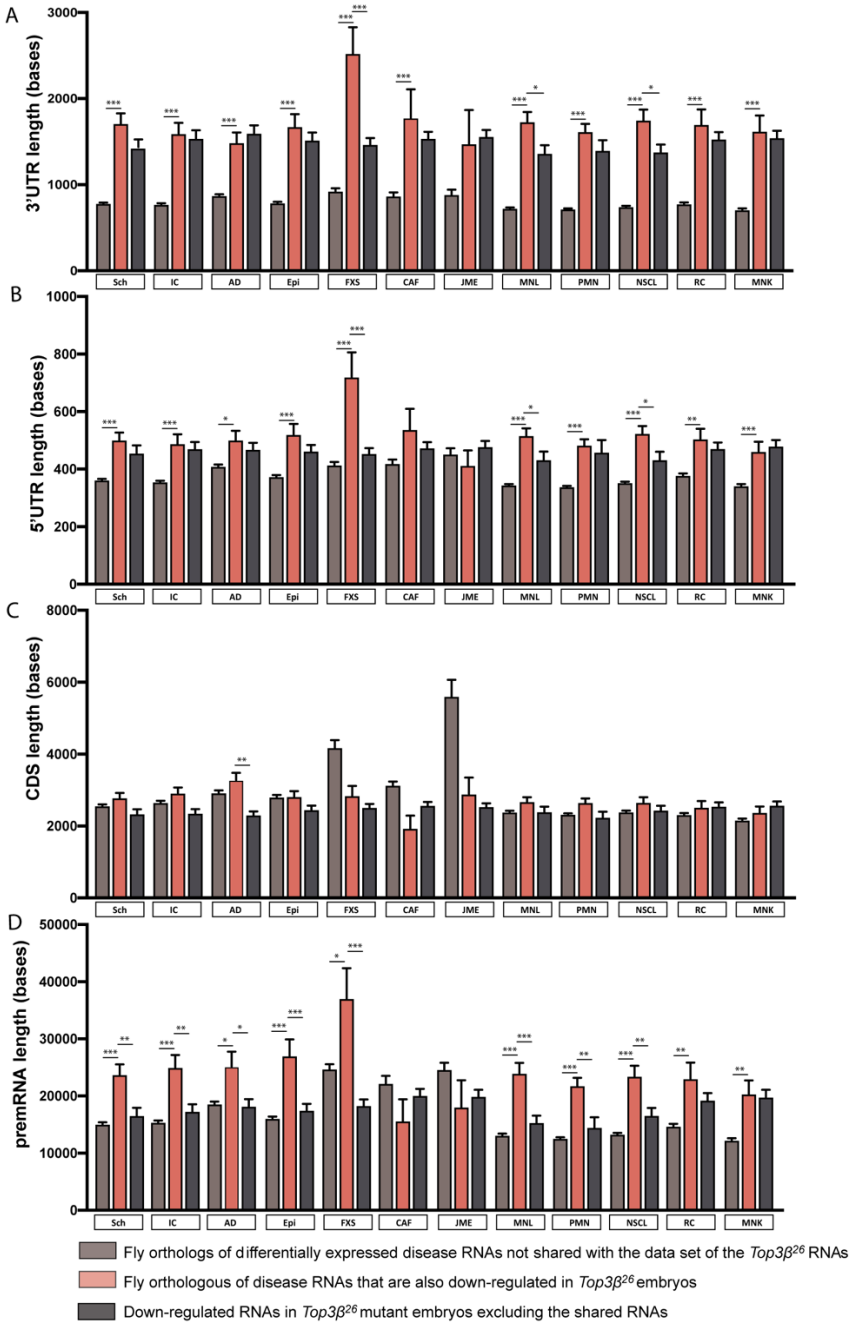

Supplementary Fig. S4: Transcript features for the differentially expressed RNAs from the embryo and the fly homologs of genes associated with the indicated diseases. A, B) mRNAs shared between the two lists show longer UTRs compared to the average fly homolog of the disease mRNA and the average *Top3β* dependent mRNA. **C)** CDS length revealed no significant difference between the three gene lists for each disease (except for AD). **D)** Shared mRNAs show longer pre-mRNAs compared to the average disease-homolog mRNA length and the average length of the embryonic *Top3β*-dependent RNA list. p-value <0.0001=****, p-value <0.001=***, p-value <0.01=**, p-value <0.05=*. Sch: Schizophrenia, IC: Impaired cognition, AD: Autistic Disorders, Epi: Epilepsy, FXS: Fragile X syndrome, CAF: Congenital anomaly of face, JME: Juvenile Myoclonic Epilepsy, MNL: Malignant neoplasm of the lung, PMN: Primary malignant neoplasm, NSCL: Non-Small Cell lung carcinoma, RC: Renal carcinoma, MNK: Malignant neoplasm of the kidney.

Figure S5

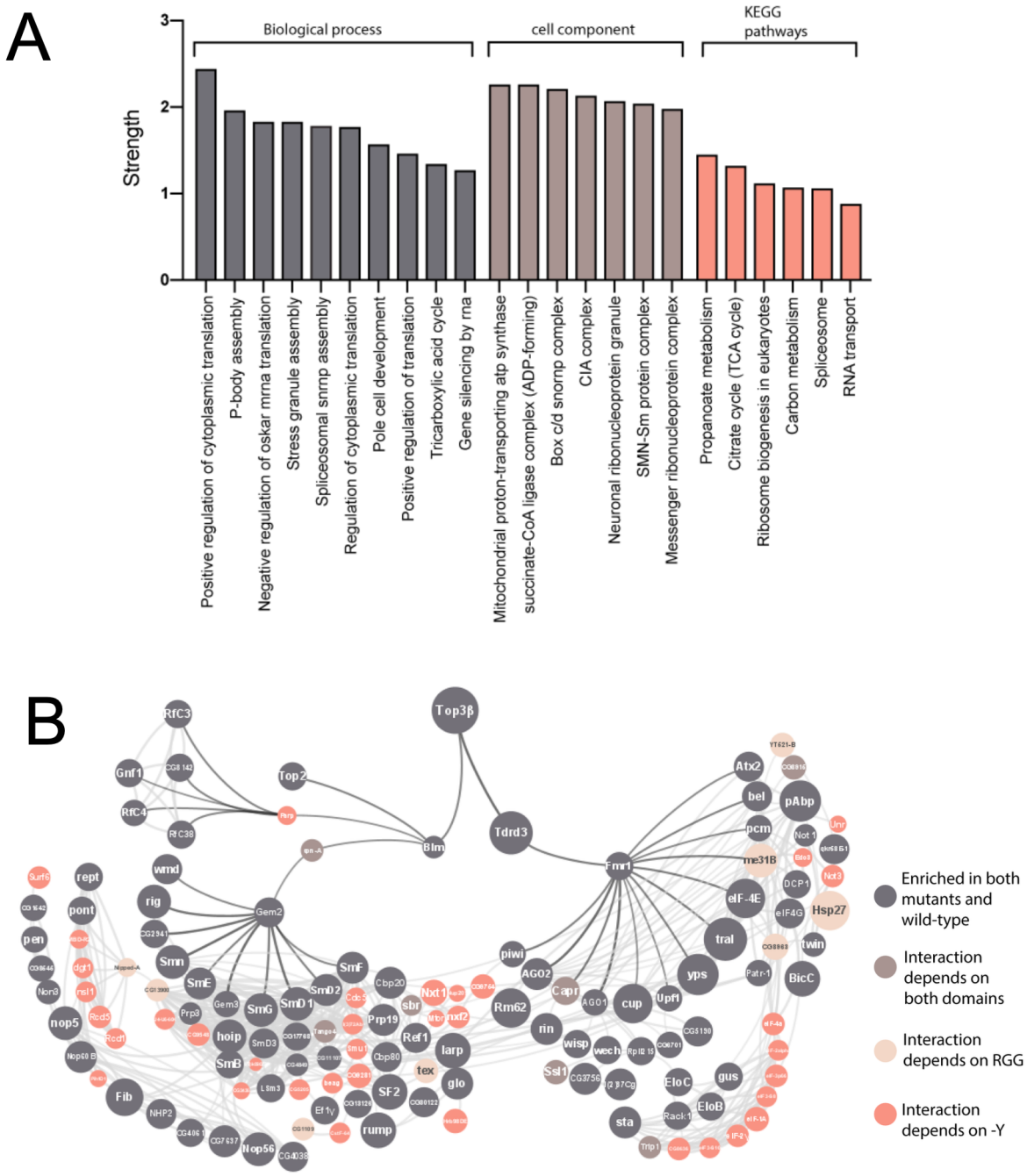

Fig. S5: Pathways and interactions of Drosophila Top3β. A) ***Gene ontology enrichment for Top3β-associated proteins for the top 100 interactors identified in embryonic extracts.*** Immunoprecipitations (IP) on extracts from 0-2 hours old embryos were performed using *Top3β-eGFP* and the *eGFP* control line. Polypeptide components of the IP complexes were analyzed using mass spectrometry (MS) and their abundance was compared to the eGFP control. This resulted in a list of 426 potential complex components with an adjusted p-value <0.01 and log2FC>1 (**Supplementary Table S5).** 89 ribosomal proteins were in this set. A gene ontology enrichment analysis was then performed for the top 100 (according to log2FC) non-ribosomal proteins. This revealed proteins involved in the activation of translation, P-bodies, stress granules, and neural ribonucleoprotein granules, all membrane-less structures involved in storing specific mRNAs during periods of stress or concentrating mRNAs and regulatory proteins (12). Additionally, the interactors were also enriched in several functions related to mitochondria. **B)** ***Proteins enriched in the embryonic protein-IP with their***

physical interactions according to Cytoscape-String. Proteins that ended up further away from Top3β than the ones shown here, were removed from the interaction map. Tdrd3, an established interactor of Top3β (13), was among the top enriched proteins, suggesting that our immunoprecipitation was specific. To assess the role of the Y332 residue and the RGG box in Top3β interactions, IP results were compared with the ones from the *Top3β* mutants *Top3β*^{Y332F}*-eGFP* and *Top3β*$^{\Delta RGG}$*-eGFP*. Among the 337 non-ribosomal binding candidates, 102 needed the Y residue and the RGG box to bind to Top3β-eGFP **(Supplementary Table S5)**. An additional 16 proteins needed the Tyr (but not the RGG) and 23 the RGG box (but not the Y332) for their binding to Top3β. A large fraction of the identified proteins is involved in RNA transport, translation, splicing, mRNA surveillance, and degradation. The physical interaction map of the proteins enriched in the Top3β::GFP IP was created using Cytoscape-String and the results from the mutant analyses were entered into this map. The resulting map resolved into two distinct sub-maps. The left branch connects Top3β functions to its nuclear functions and includes splicing factors. The right branch is enriched in cytoplasmic proteins and includes Tdrd3, FMR1, the piRNA pathway, and translation. The association first Tdrd3 and FMRP has already been described from work with vertebrate cell cultures (74). The interaction of Me31B with Top3β turned out to be dependent on the RGG box. As an RNA helicase, Me31B is a core component of a variety of ribonucleoprotein complexes (RNPs) that participate in translational control and mRNA decapping during embryogenesis, oogenesis, neurogenesis, and neurotransmission (14)(15)(16)(17)(18)(19)(20)(21). Me31B RNPs also containing Tral, eIF4E1, Cup, and pAbp. They are also involved in RNA localization and translational control of maternal mRNAs during oogenesis and embryogenesis (18). These other complex proteins were also enriched in the embryonic Top3β::eGFP IP.